Winds of opportunity

The effects of wind on intertidal flat accretion

Colosimo, Irene; van Maren, Dirk Sebastiaan; de Vet, Paul Lodewijk Maria; Winterwerp, Johan Christiaan; van Prooijen, Bram Christiaan

DOI
10.1016/j.geomorph.2023.108840

Publication date
2023

Document Version
Final published version

Published in
Geomorphology

Citation (APA)
Colosimo, I., van Maren, D. S., de Vet, P. L. M., Winterwerp, J. C., & van Prooijen, B. C. (2023). Winds of opportunity: The effects of wind on intertidal flat accretion. *Geomorphology*, *439*, Article 108840. https://doi.org/10.1016/j.geomorph.2023.108840

Geomorphology 439 (2023) 108840

Contents lists available at ScienceDirect

Geomorphology

journal homepage: www.journals.elsevier.com/geomorphology

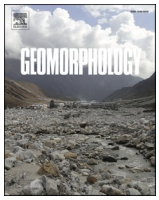

Winds of opportunity: The effects of wind on intertidal flat accretion

Irene Colosimo [a], Dirk Sebastiaan van Maren [a,b,c,*], Paul Lodewijk Maria de Vet [a,c], Johan Christiaan Winterwerp [a], Bram Christiaan van Prooijen [a]

[a] Delft University of Technology, Stevinweg 1, Delft, 2600, AA, the Netherlands
[b] State Key Laboratory of Estuarine and Coastal Research, No. 500, Dongchuan Road, Shanghai 200241, China
[c] Deltares, Boussinesqweg 1, Delft, 2600, MH, the Netherlands

ARTICLE INFO

Keywords:
Intertidal flats
Wind-driven transport
Suspended sediment concentration
Coastal morphology
Deposition
Over-consolidation
Accretion

ABSTRACT

Intertidal ecosystems are threatened by sea level rise and anthropogenic pressures. Understanding the processes controlling the morphodynamic developments of tidal flats is crucial for sustainable management of these systems. Analysis of three extensive fieldwork campaigns carried out on two adjacent mudflats fringing the Dutch Western Wadden Sea (from 2016 to 2018) provides important new insights into the conditions controlling a permanent increase of tidal flat elevation ('accretion'), in which the wind and consolidation processes play a pivotal role. Sediment temporarily settles ('deposition') on the flats during a period of high suspended sediment availability and water level setup (often following a storm). A tidal flat accretes when a new layer of sediment over-consolidates: a state in which the bed strength is much larger than it would attain during inundated conditions, due to high stresses experienced during prolonged drying. This happens when a phase of sediment deposition is followed by a sufficiently long period with a low ambient water table (phreatic level) and aerial exposure. The chronological order of sediment deposition and over-consolidation provides a window of opportunity for tidal flat accretion. Such a window of opportunity depends on the hydrodynamic forcing (tides, waves, wind), on the consolidation state of the bed, and on sediment availability. Wind plays a crucial role in creating the conditions for tidal flat accretion because the wind direction influences the duration of a low water table and aerial exposure and therefore (over-)consolidation rates, which we refer to as the 'winds of opportunity'. An abundance of sediment may even limit tidal flat accretion, because large deposition rates substantially increase consolidation timescales.

1. Introduction

Intertidal flats are valuable ecosystems, providing habitat for a wide variety of benthic species, which are in turn vital for higher trophic species such as birds (Barbier et al., 2011). At the same time, intertidal flats in combination with their supratidal salt marshes dissipate energy resulting from waves and currents, providing a natural barrier protecting inland areas (Yang et al., 2012; Möller et al., 2014; Zhu et al., 2020; Temmerman et al., 2023) that may keep pace with sea level rise (Kirwan et al., 2016). However, many intertidal flats are at risk of drowning due to (accelerated) sea level rise (e.g. Reed, 1995; Kirwan and Megonigal, 2013; Timmerman et al., 2021) and land subsidence. The resilience of these systems is also degraded by other human activities, like land reclamation (Zhang et al., 2021) and interventions causing reduction of sediment supply to river deltas (Yang et al., 2003a; Syvitski et al., 2005; Li et al., 2020; Yang et al., 2020; Dethier et al., 2022). These increasing anthropogenic pressures, in combination with the high environmental value of these ecosystems and their role in shoreline protection, fuels the need to thoroughly understand the biogeomorphodynamics of tidal flats.

Predicting the morphological evolution of intertidal systems is complex, partly due to the variability in timescales that control sedimentation and erosion, ranging from intra-tidal to seasonal timescales (Yang et al., 2012; Sassi et al., 2015). At the intra-tidal timescale, sediment deposits around high water slack, when the flow is weak and the wave-induced resuspension rates are low. This has been especially observed at intertidal flats bordering macro-tidal estuaries where slack water conditions last several hours (e.g. Deloffre et al., 2007). In micro-to-*meso* tidal systems, this intratidal variability in wave-induced resuspension is smaller because of smaller fluctuations in the water depth. In these systems the very shallow water depths (smaller than 20–25 cm) represent conditions with the largest changes in bed level (Shi et al., 2017a; Zhu et al., 2017). On the Jiangsu coast (China) changes in bed

* Corresponding author at: Deltares, Boussinesqweg 1, Delft, 2600, MH, the Netherlands.
E-mail address: bas.vanmaren@deltares.nl (D.S. van Maren).

https://doi.org/10.1016/j.geomorph.2023.108840
Received 29 March 2023; Received in revised form 19 July 2023; Accepted 20 July 2023
Available online 26 July 2023

level during such conditions contribute up to 33 % of the changes over a full tidal cycle (Shi et al., 2017a). At seasonal timescales, the alternation of storm and fair weather dictates the changes in bed elevation (Yang et al., 2003b, 2008; Fan et al., 2006; Belliard et al., 2019), with storms resulting in erosion (Yang et al., 2023a) but also in relatively large sedimentation (Turner et al., 2006; Li et al., 2015). Superimposed on seasonal effects resulting from wave energy are the effects of biota (Le Hir et al., 2007). In muddy areas algae mats may reduce erosion rates in summer due to strengthening of the bed (Kornman and Deckere, 1998; Paterson and Hagerthey, 2001) but also because bedforms and therefore bed roughness is smaller (Malarkey et al., 2015; Parsons et al., 2016). Erosion can also be enhanced by biota by making sediment available for erosion or modifying the critical shear stress for erosion (Van Prooijen and Winterwerp, 2010; Orvain et al., 2012).

Where the erosion of sandy beds mainly depends on the hydrodynamic forcing and grain size, erosion of muddy or mixed sand-mud beds is more complex. In sand-mud mixtures the mud content influences erodibility of the bed, especially influencing the critical shear strength against erosion (Mitchener and Torfs, 1996; Van Ledden et al., 2004; van Rijn, 2020). Selective erosion of different particles may also lead to armouring (Sanford, 2008; Le Hir et al., 2011) which may lead to vertical layering of sandy and muddy deposits (Fan and Li, 2002; Fan et al., 2002). The substrate also influences development of biota which in turn leads to preferential development of a muddy or sandy substrate (Garwood et al., 2015). Crucial to muddy environments is that at a sufficiently high mud content the density and permeability of the sand-mud mixture will vary over time through consolidation processes (Torfs et al., 1996; van Rijn and Barth, 2019) influencing the shear stress of the bed and therefore influencing its resistance against erosion over time.

In submerged conditions, sediment consolidation is driven by the reduced gravity of the sediment bed (determined by the difference in density between sediment bed and water) controlling the consolidation rate (Been and Sills, 1981). Pore water is expelled by the weight of the consolidating sediment bed resulting in particle rearrangement and compaction (decreasing the bed porosity and thickness, while increasing the bulk density) - see e.g. Merckelbach and Kranenburg (2004). A submerged sediment bed consolidating under its own weight only slowly develops shear strength and therefore resistance against erosion (for instance during storm events). However, when a tidal flat emerges, it becomes also subject to vertical compaction driven by capillary suction (Winterwerp et al., 2021). This under-pressure is generated by a lowering of the phreatic level within the mudflat bed driven by the falling tide. The suction head (i.e. the difference between bed level and phreatic level) increases with bed elevation due to the asymmetry in ingress and egress of pore water across the tidal flat (Riedel et al., 2010). As a result, the sediment bed becomes over-consolidated (the bed is more consolidated than could be expected from self-consolidation). The shear strength of the bed is high resulting from larger pressures experienced in the past. The contribution of this phenomenon to bed compaction is crucial, as under-pressures induce stresses in the upper parts of the bed which are orders of magnitude larger than the self-weight stresses by reduced gravity (Winterwerp et al., 2021).

The section above illustrates how bed emergence influences consolidation rates and hence shear strength of the sediment bed. This implies that the erosion rates of intertidal areas (e.g. during during storm conditions) is strongly influenced by its inundation history, especially the duration for which the flat is emerged. And although many studies have addressed the morphodynamic behaviour of intertidal areas (Janssen-Stelder, 2000; Allen and Duffy, 1998; Bassoullet et al., 2000; Green et al., 2000; Hir et al., 2000; Zhu et al., 2017; Shi et al., 2012, 2017a), no systematic studies have been executed investigating morphodynamic changes of the bed in response to inundation history. Especially in microtidal environments (with a tidal range <2 m) the inundation history may be strongly influenced by meteorological conditions due to storm setup or setdown.

An example of such a microtidal environment is the Dutch Wadden Sea. The tidal range in the Western Wadden Sea is <2 m, while the annually recurring storm surge is 1.88 m (Vuik et al., 2018) and periods with storm set-down also regularly occur (not yet documented in literature). Winds have a pronounced impact on the residual water flux through the basin (Duran-Matute et al., 2014, 2016; Sassi et al., 2016). Large parts of the Western Wadden Sea are very muddy (Colosimo et al., 2020; Colina Alonso et al., 2021), therefore providing an example of a system where (1) meteorological effects strongly influence the residual flow as well as inundation frequency and period and (2) erosion processes are influenced by consolidation of the bed. This study aims to advance our understanding of the morphodynamics in this microtidal storm-influenced environment by analyzing in detail the hydrodynamic and sedimentary processes over a muddy tidal flat. For this purpose we have collected detailed field observations at four sites during contrasting meteorological conditions covering winter and spring time periods.

2. Material and methods

2.1. Study area

The Dutch Wadden Sea is the world's largest uninterrupted system of tidal flats and barriers, of which the natural dynamics are increasingly constrained by human interventions (Elias et al., 2012). The larger part of its various tidal basins are predominantly sandy, whereas the tidal flats are very muddy (Colina Alonso et al., 2021). Fine-grained sediments are provided by the adjacent North Sea, with dominant westerly winds driving a residual transport of fines from west to east through its main channels (Nauw et al., 2014; Sassi et al., 2015). This westward flow and transport component is probably even more pronounced along the tidal flats fringing the main coastline (Colosimo et al., 2020) and the tidal divides separating the main land from the barrier islands (van Weerdenburg et al., 2021). The coastal lagoon is sheltered from North-Sea swells by barrier islands, and therefore waves are mainly locally generated and have a relatively short period. Despite being mainly locally generated, these waves are important for resuspending fine-grained sediment (Ridderinkhof et al., 2000; Janssen-Stelder, 2000; Colosimo et al., 2020).

We investigate two adjacent intertidal flats fringing the mainland coast of the Dutch Wadden Sea (Fig. 1): Koehool (K) and Westhoek (W) (Fig. 1[b]). Tides from the North Sea come into the basin via a branching channel system, leading to flooding and drying of the intertidal areas. The Kimstergat tidal channel, oriented parallel to the coast, connects Harlingen Harbour area to the investigated flats (Fig. 1[b]). The channel influences the local hydrodynamics, inducing a mainly long-shore directed flow onto the neighbouring flats and marshes (Colosimo et al., 2020).

Koehool and Westhoek were selected in a larger scale project as contrasting areas, as marshes are present at Westhoek, while they are absent at Koehool. Koehool tidal flat is situated in proximity of the north-east edge of the Kimstergat tidal channel and presents one order of magnitude larger slope (0.0016 %) than the contiguous Westhoek flat (0.0007 %) (Fig. 1[d].

Two sites along each transect were investigated, with the aim of covering both the higher (KH, WH) and the lower (KL, WL) intertidal areas, see Fig. 1[c]) and Table 1.

More specifically, as we aimed at understanding the mechanisms controlling the intertidal flat morphodynamics at different bed elevations, we carried out measurements close to the tidal channel (site KL, −1 mMSL), at the foreshore of the saltmarshes area (site WH, +10 m MSL) and at two sites having relatively similar bed elevations (−0.13 mMSL KH and − 0.30 m MSL WL) but very different in grain size (30 μm at KH vs 99 μm at KL), sited at different distances from the shoreline (430 m KH vs 1700 m WL)- see Table 1.

The elevation of the two tidal flats significantly increased during the last century (Baptist et al., 2019): ~1.5 m accretion at Koehool and ~2.5 m at Westhoek. Since the 1990's, sediment deposition at Westhoek was

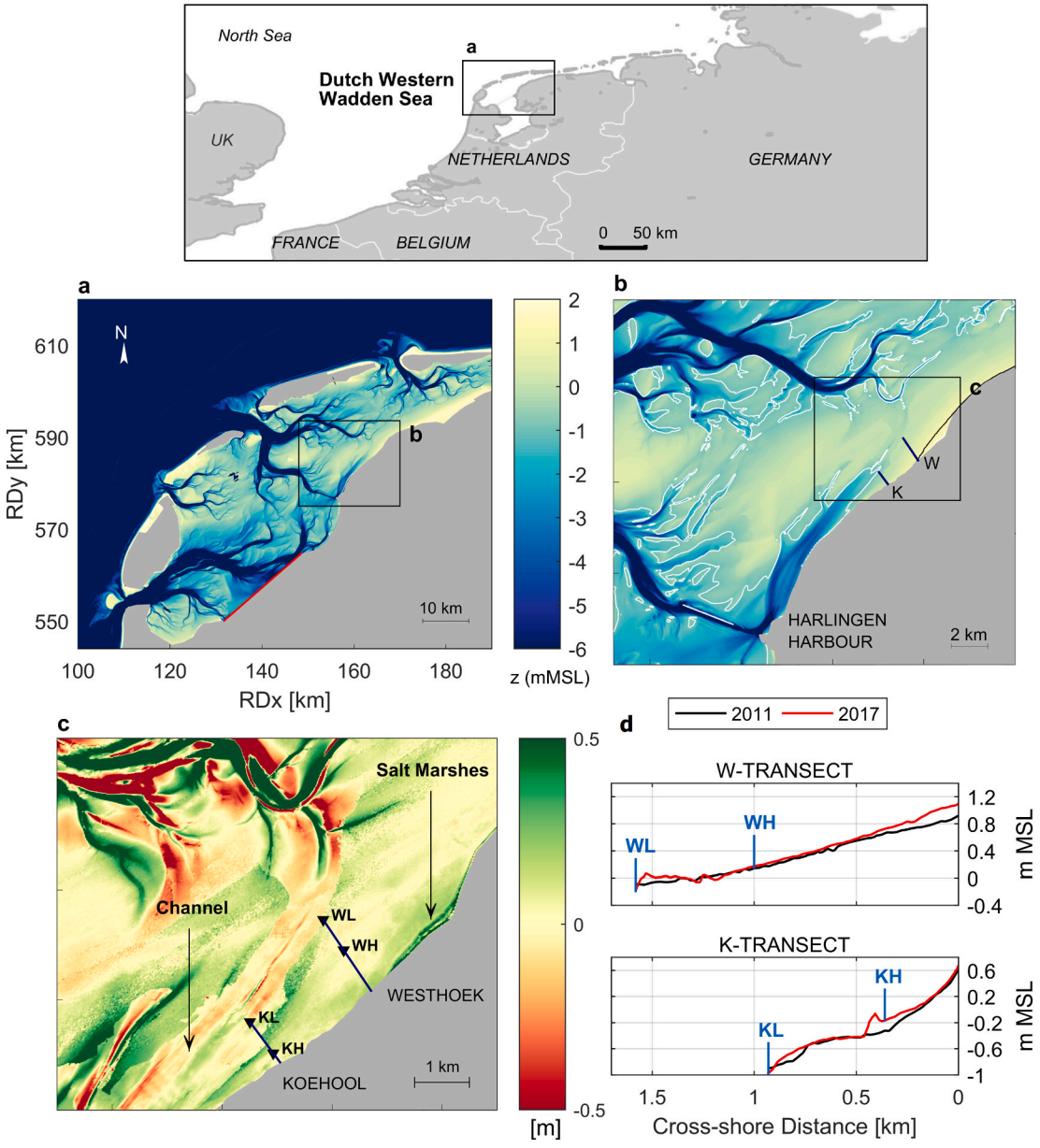

Fig. 1. Top panel indicates the position of the Dutch Western Wadden Sea with respect to other European countries; panel [a] shows the 2017 Dutch Western Wadden Sea bathymetry with grey colour indicating the barrier islands and land. The closure dam (Afsluitdijk) is indicated in red. The two investigated "K" and "W" transects (panel b) refer to the tidal flats of Koehool and Westhoek, respectively. Net bed level changes over the period 2011–2017 are provided in panel c, (with positive values indicating increase in bed elevation). Two sites per transect were monitored, indicated as KL, KH, WL and WH (panel d, where 'L' and 'H' refer to lower and higher mudflat, respectively). The bed levels of the two transects are provided for both 2011 and 2017 (note that the y-axis is different because transect W is higher elevated, but the interval 1.8 m is the same in both sub-figures). (For interpretation of the references to colour in this figure legend, the reader is referred to the web version of this article.)

followed by salt marsh development (nowadays having a maximum width of 160 m), whereas the low-lying Koehool tidal flat remains unvegetated. This rapid accretion was triggered by a closure dam (Afsluitdijk, indicated by a red line in Fig. 1[a]) constructed in the early 1930's (Elias et al., 2012; Colina Alonso et al., 2021) which is to date controlling persistent deposition of fine-grained sediments (Van Maren et al., 2023). Fig. 1[c] shows the bed level accretion and degradation over a 6-year period (2011–2017). The bed level at both Westhoek and at Koehool accreted (Fig. 1[d]). At Westhoek the maximum bed level increase (~20 cm) occurred in proximity of the most elevated salt-marshes (from 0.9 mMSL to 1.13 mMSL, with"mMSL" indicating"-meters above Mean Sea Level"). Along the Koehool transect sedimentation of 0.3 m was observed at 0.4 km from the coastline (from −0.4 mMSL to −0.1 mMSL).

2.2. Field measurements

Field measurements were carried out to capture the hydrodynamic and sediment transport mechanisms affecting the short-term morphology of intertidal flats. Field campaigns were carried out during spring (April–May) 2016 (Koehool) and 2017 (Westhoek), and in the winter period, from December 2017 to February 2018, at Koehool and Westhoek simultaneously. This campaign's design allowed a comparison of intertidal flat short-term morphodynamics during fair and severe weather conditions.

Bed level changes, suspended sediment concentrations, currents,

Table 1
Bed elevations (z_b), median grain size (d_{50}), distance from shore and periods of measurement at the four investigated sites: KL, KH, WL, WH. The distance from the shore refer to the winter period; during spring the difference in the frame positioning varied of 30–50 m. This difference is not accounted for in the analysis, as at such short distance differences in hydrodynnamics or sediment transport are not significant. The bed sediment grain size is measured by analyzing a grab sample representing the top 5 cm of the sediment bed with laser diffraction (using a Malvern Mastersizer).

Site	z_b	Grain Size	Dist. from shore	Period
K_L	MSL-1 m	123 μm	0.97 km	Apr-May2016, Dec2017-Feb2018
K_H	MSL-13 cm	30 μm	0.43 km	Apr-May2016, Dec2017-Feb2018
W_L	MSL-20 cm	99 μm	1 km	Apr-May2017, Dec2017-Feb2018
W_H	MSL + 10 cm	13 μm	1.7 km	Apr-May2017, Dec2017-Feb2018

waves and water levels were obtained through instrumentation that have been largely used in coastal environments (e.g. Andersen and Pejrup, 2001; Hoitink and Hoekstra, 2005; Downing, 2006; Andersen et al., 2006; Zhu et al., 2014; Shi et al., 2015; Elias et al., 2019; de Vet et al., 2020; van Prooijen et al., 2020; Pearson et al., 2021). Two equipped frames were placed in the intertidal area across each investigated transect. The deployed measuring frames contained one or two Acoustic Doppler Velocimeters (ADV, Nortek), one or more (up to three) Optical Back Scatters (Optical Back Scatter Campbell3+), and one Acoustic Doppler Current Profiler (Aquadopp Profiler, ADCP, Nortek). Moreover, one Wave Logger (OSSI-010-003C, Ocean Sensor System) was installed in the proximity of each frame. In the following, the specific use of each instrumentation is detailed.

The ADVs measured the flow velocity at ~20 cm above the bed (hereafter indicated as"cmab") with a frequency of 8 Hz, either continuously or in burst intervals of 5–20 min. The sensor positioning at 20 cmab has been selected based on previous in-situ studies conducted in intertidal environments (e.g. Andersen and Pejrup, 2001; Zhu et al., 2014; de Vet et al., 2020). This distance allows a long-enough submergence of the sensor and ensures, at the same time, that the sensor is not buried during depositional events. The Nortek ADVs measure the distance between the probe and a solid wall (the bed) at the beginning and at the end of a burst (Zhu et al., 2017) with an accuracy around 1 mm (Shi et al., 2015). The bed level change signals were smoothed using a 40 min running mean.

The ADCPs measured 3D flow velocity over the full water depth. The instruments were installed upward-looking, with the acoustic transmitter as close as possible to the bed. The distance of the lower measurement volume from the bed was about 25 cm, given by the sum of the sensors distance from the bed (on average 15 cm) and a default blanking distance of 10 cm.

The OBS is an optical sensor measuring turbidity by detecting infrared light scattered from suspended matter (Downing, 2006). Multiple OBS sensors, from which the Suspended Sediment Concentration (SSC) were deduced, were installed at different elevations above the bed. During all field campaigns and at all locations, one OBS was installed at ~20 cmab (i.e. flow velocity and SSC were measured at the same distance from the bed). In 2017 and 2018 additional OBS sensors were installed at ~60 cmab, whereas at the site KL (the lowest site) a third OBS was deployed at ~120 cmab, to capture the sediment concentration gradients along the water depth.

All publicly available data was provided by the Dutch Ministry of Public Works (Rijkswaterstaat). This includes the actual and the astronomical water levels measured at a tidal gauge station in the Port of Harlingen, bathymetry maps (Vaklodingen dataset), and wind data (measured hourly at the meteorological station of Leeuwarden, ~20 km distance from the study area). Water levels and bathymetric data are relative to the mean sea level.

2.3. Data processing

The Wave Logger pressure signal, and the pressure signal from the ADVs and the ADCPs were corrected from air pressure variations using the data from the meteorological station of Leeuwarden (~20 km distance from the measuring area).

The ADV velocity data was filtered by applying a threshold values of 70 % for beam correlation and 100 counts for signal amplitude. In this way, erroneous data (e.g. during emergence of the instrument) are removed. The remaining ADV flow velocity data have been despiked using the methodology proposed by Goring and Nikora (2002).

Wave parameters were computed from the ADV pressure and flow velocity signals using a wave-directional spectral analysis, following Tucker and Pitt (2001). The flow velocities recorded by the ADV were combined with the wave data recorded by the wave logger to compute a combined bed shear stress using the WCI method of Soulsby (1995) - see Colosimo et al. (2020) for details.

The OBS sensors were calibrated in the laboratory using in-situ collected sediment-laden water samples. The calibration procedure in laboratory included synchronized OBS measurements (in a 8 l calibration bowl) and sample filtration through 0.45 μm pore filters. From 20 to 30 dilution steps were executed for concentrations between 0 and 10 g/l. At each calibration step the SSC was measured using the OBS, and a 50 ml water sample was collected and filtered on a pre-weighted filter and oven-dried for 24 h at 105 °C. The filters have been hence weighted again, to determine the sediment mass contained in each sample. The resulting calibration curve was used to convert the OBS signal (voltage) into a sediment concentration. For the full range between 0 and 10 g/l the 15 OBS sensors follow a non-linear relationship best approximated with a quadratic fit, resulting in R^2 values between 0.86 and 0.96 (with an average R^2 of 0.91). Up to a concentration of 3 g/l (covering the vast majority of time) SSC was linearly scaling with the OBS signal.

This calibration procedure method, including water samples and subsequent filtration, has been also applied for SSC measurements in the Wadden Sea channels (Nauw et al., 2014; Gerkema et al., 2014; van der Hout et al., 2015; Pearson et al., 2021, e.g.) and intertidal flats (Baeye et al., 2011; Hache et al., 2019, e.g.) and is considered among the most reliable measure to give the correct sediment concentration (Bundgaard and Lumborg, 2019).

3. Results

3.1. Bed level changes over tidal to yearly timescales

Over a 6-years time period, the maximum bed level increase measured 20 cm at Westhoek and 30 cm at Koehool (Fig. 1[d]), implying a yearly-averaged (maximum) bed level increase of ~3 cm and ~5 cm, respectively. Throughout this paper we will refer to the settling of particles on the bed as *sedimentation* or *deposition*, whereas a net increase in the bed level over longer timescales is referred to as *accretion*.

At monthly timescales, similar magnitudes in net changes are observed using the ADV bed level observations (Fig. 2). Over the two-months winter measurement period, the bed erodes at all observation stations. Along each transect, the net erosion is larger at the seaward location compared to the landward location: −0.3 cm and -4.5 cm (respectively) at KH and KL (Koehool transect); −1.9 cm and -3.1 cm (respectively) at WH and WL (Westhoek transect) - all well within the accuracy range of the ADV (Shi et al., 2015). Over the one-month spring measurement period the bed elevation was rather stable at KL, with a few episodes of sediment deposition around May 15, resulting in a bed level increase of ~2 cm, directly followed by erosion. In contrast, site KH experienced a net accretion of 7.4 cm.

The cumulative sedimentation and erosion per site (Fig. 2) reveals

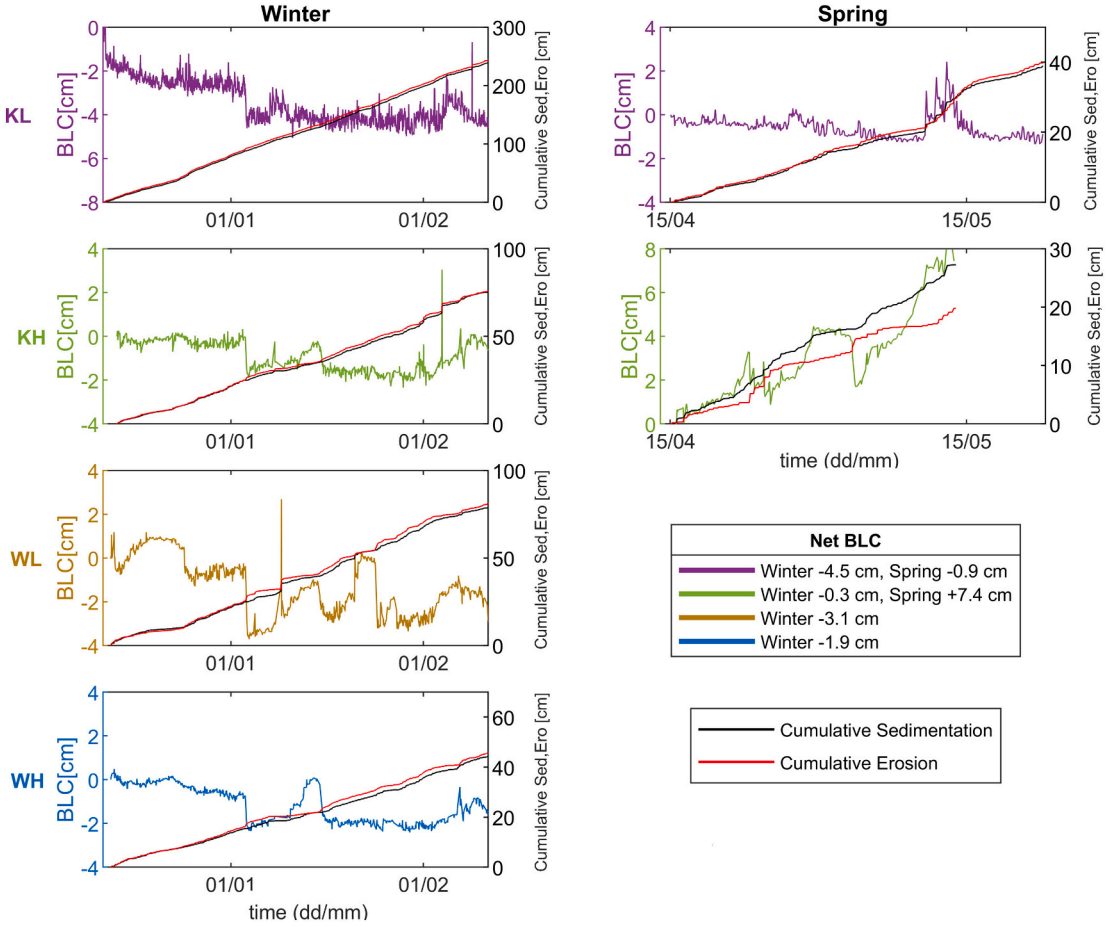

Fig. 2. Bed levels (BLC, left panel) and cumulative erosion/deposition (right axes) measured in winter (left panels) and spring (right panels) for the four observation stations. One event with 16 cm deposition on January 8 is excluded from site KH (discussed in detail in Section 3.3.) Cumulative deposition is defined as the summation of bed level increase (and cumulative erosion the summation of bed level decrease). With bed level data available at 40-minute intervals this differentiation represents tidal variability but not short-term variability resulting from e.g. turbulent fluctuations.

how bed variability varies over space and time. The bed variability decreases with bed elevation: the cumulative sedimentation and erosion are lowest at the most elevated site WH (45 cm in winter) and highest at the lowest site KL (250 cm in winter, 40 cm in spring), with intermediate values around mid-flat (WL and KH, both 80 cm in winter and 25 cm for KH in spring). The bed is most dynamic in winter. The lower flat (KL) is about 3 times more dynamic in winter compared to spring: both the cumulative (gross) sedimentation and erosion equal ~250 cm in two winter months and ~40 cm in one spring month. The higher flat (KH) is about 1.5 times more dynamic in winter compared to spring: the cumulative sedimentation is ~80 cm in two winter months and ~25 cm in one spring month.

Over tidal timescales, the largest net bed level changes (both deposition and erosion) occur at relatively small bed shear stress (1–1.5 Pa) - see Fig. 3. Surprisingly, large erosion rates are not related to large bed shear stresses (4–12 Pa) which typically result from wind speeds above 10 m/s (top right in Fig. 3). Another important observation is that the bed level changes on tidal timescale decreases up flat, while bed shear stresses increase up flat (Fig. 3, left panels).

3.2. Storm-induced erosion and post-storm recovery

Two different erosion types can be observed in the dataset. First, during periods with weak–to–moderate winds (u10 < 10 m/s) – mainly occurring during Eastern winds – the bed shear stresses are fairly low (maximum 1–3 Pa, depending on the site); these conditions result in sediment deposition (I.e. bed level increase) but also in relatively large bed erosion (up to 2 cm/tide, as already found in Fig. 3, right panels). The large erosion rates at relatively small bed shear stress suggest that the bed is poorly consolidated. This type of erosion (rapid erosion of poorly consolidated material at low bed shear stress) becomes more prominent in upflat direction (as also suggested by the tide-averaged analysis in Fig. 3).

The second erosion type occurs during periods with relatively strong winds ($u_{10} > 10$ m/s, mainly during Western winds) which lead to bed shear stresses larger than 1.5 Pa (and up to 12 Pa). Erosion rates are large during storm events ('Storm1' resulted in bed erosion of 1–3.5 cm over the flats; see Fig. 4). Such erosion events have a long-lasting effect (weeks/months) because the sediment deposited after the storm is easily eroded, as will be evaluated hereafter.

Post-storm sediment deposition rates are large: at KL, for instance, the bed elevation increases by 1.5–2 cm during 2–3 days of Eastern wind (January 9–11 and Feb 4–6 with u_{10} up to 15 m/s). In both cases the freshly deposited sediment is eroded again at relatively small bed shear stress (< 1 Pa), resulting in an elevation setback corresponding to the post-storm elevation. At site KL, the bed does not even recover from the storm–induced erosion over the whole subsequent measurement period. At higher bed elevations (sites WL, KH and WH), the bed recovers on average by 95 % within the 12 days following the storm (January 3–15), with highest deposition rates (up to 0.5 cm/tidal cycle) occurring during Eastern wind (January 7–15). But also for these higher sites the strength of the bed is weaker than before the storm. An event with a relatively small bed shear stress (1–3 Pa on January 16) occurring directly after the sediment deposition period, completely eroded the bed back to its post-

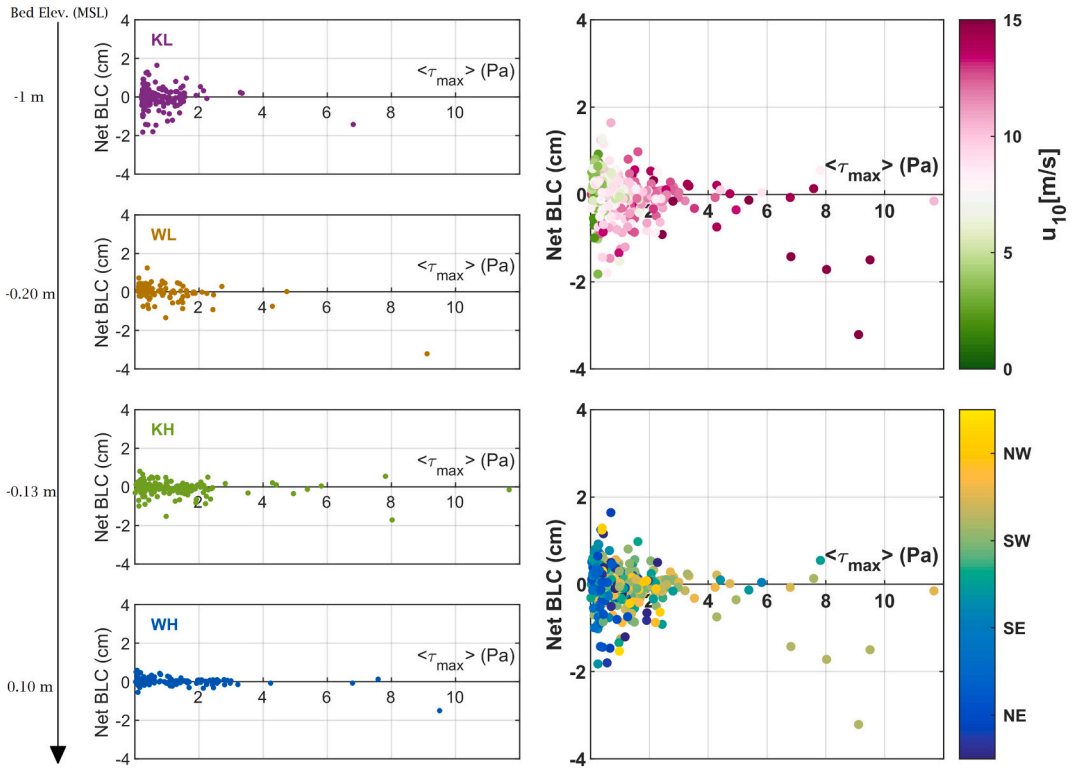

Fig. 3. Net bed level changes (BLC) per tidal cycle (one marker represents one tidal cycle) as a function of tide-averaged maximum bed shear stress at each site (left panels). The right panels include the net BLC measured at all sites. Upper right panel: BLC as a function of tide-averaged maximum bed shear stress and wind speed; lower right panel: BLC as a function of tide-averaged maximum bed shear stress and wind direction. The combined wave-current bed shear stress has been computed using (Soulsby, 1995)'s method.

storm level, similar to KL. During the second storm (January 18, 'Storm 2'), western winds up to 21 m/s resulted in bed shear stresses up to 10 Pa but, even under such high bed shear stress none of the sites exhibited erosion. The bed level at all sites remained at the bed level attained after the erosion event of January 16, i.e. approximately the bed elevation after 'Storm 1'.

These observations indicate that storms erode the bed until a level in which the strength of the bed is too large to erode further. Post-storm sediment deposition is large but the strength of these fresh deposits is low. Rapid erosion of the post-storm sediment deposits follows, even during periods of relatively small bed shear stress. No new equilibrium with a stable bed was attained within the observational periods. We hypothesize that such a new equilibrium can be reached after sufficiently long periods of emergence, as will be explained in more detail in Section 3.5.

3.3. Deposition events

Deposition rates are highest during two specific events: the passage of highly concentrated turbid fringes and fluid mud formation. Their impact on deposition rates will be investigated in more detail below, using observations on intratidal timescales.

3.3.1. Depositional turbid fringes

A satellite picture (September 23, 2017) shows a turbid band near the study area (Fig. 5). Highly turbid zones are noticed especially at the intertidal areas surrounding the Kimstergat tidal channel. Such turbid bands result in sharp peaks in the SSC typically occurring at the beginning and/or at the end of a submergence period. They are referred to as turbid fringes (Green, 2003). In the Wadden Sea, such turbid fringes are particularly observed when calm weather conditions follow relatively energetic tides with considerable wave-induced resuspension. As such they are more common in the more energetic fall/winter period. We will further explore the role of the turbid fringe by examining a period in our dataset (January 10, Fig. 6) with meteorological conditions very similar to those in Fig. 5 (southern wind with speed lower than 5 m/s).

The tides are asymmetric with a shorter rising stage than falling stage resulting from the shallow water depth (especially at water depths below 20 cm, which is not recorded by the instruments). As a result the suspended sediment concentration SSC peaks up to 3 g/l shortly after inundation, and rapidly decreases in concert with the rising bed levels (Fig. 6), suggesting the passage of a depositional turbid fringe. Deposition rates during the passage of the turbid fringe were larger at Westhoek compared to Koehool: 0.45 cm in 1 h (i.e. 0.45 cm/h) at WH, 0.44 cm in 1 h and 32 min (i.e. 0,28 cm/h) at WL and 0.36 cm in 2 h and 22 min (i.e. 0.15 cm/h) at KH. Throughout our dataset, sediment deposition rates are up to 2 cm/tide in winter and 1.3 cm/tide in spring. During the following ebb, these deposits were negligibly resuspended by the weaker flow (below 0.2 m/s). The vertical OBS array at KH and WL reveal pronounced sediment stratification with SSC at 60 cmab (up to 1.5 g/l) about 30–50 % smaller compared to SSC at 20 cmab (up to 3 g/l).

In order to understand how the sediment concentration at such turbid fringes relates to the stresses at the bed, we further analyse depositional events resulting in deposition rates exceeding 0.4 cm/tide, using Fig. 7. The suspended sediment concentrations show a stronger correlation with flow velocity u_h (high SSC at high u_h) than with the wave orbital velocity u_{orb} (highest SSC actually occurring during periods of low u_{orb}). At all sites the largest SSC is observed at the smallest water depths (especially < 0.25 m) indicating the existence of concentrated turbid fringes at the tidal wave front. SSC peaks occur at the beginning of the flood (when flow velocities are highest), except for site KL (closest to the tidal channel) where ebb and flood concentrations are comparable. The observations in Fig. 6 also indicate that at site KL the turbid fringe has a smaller effect on bed elevation. Apparently, the largest SSC (i.e. the

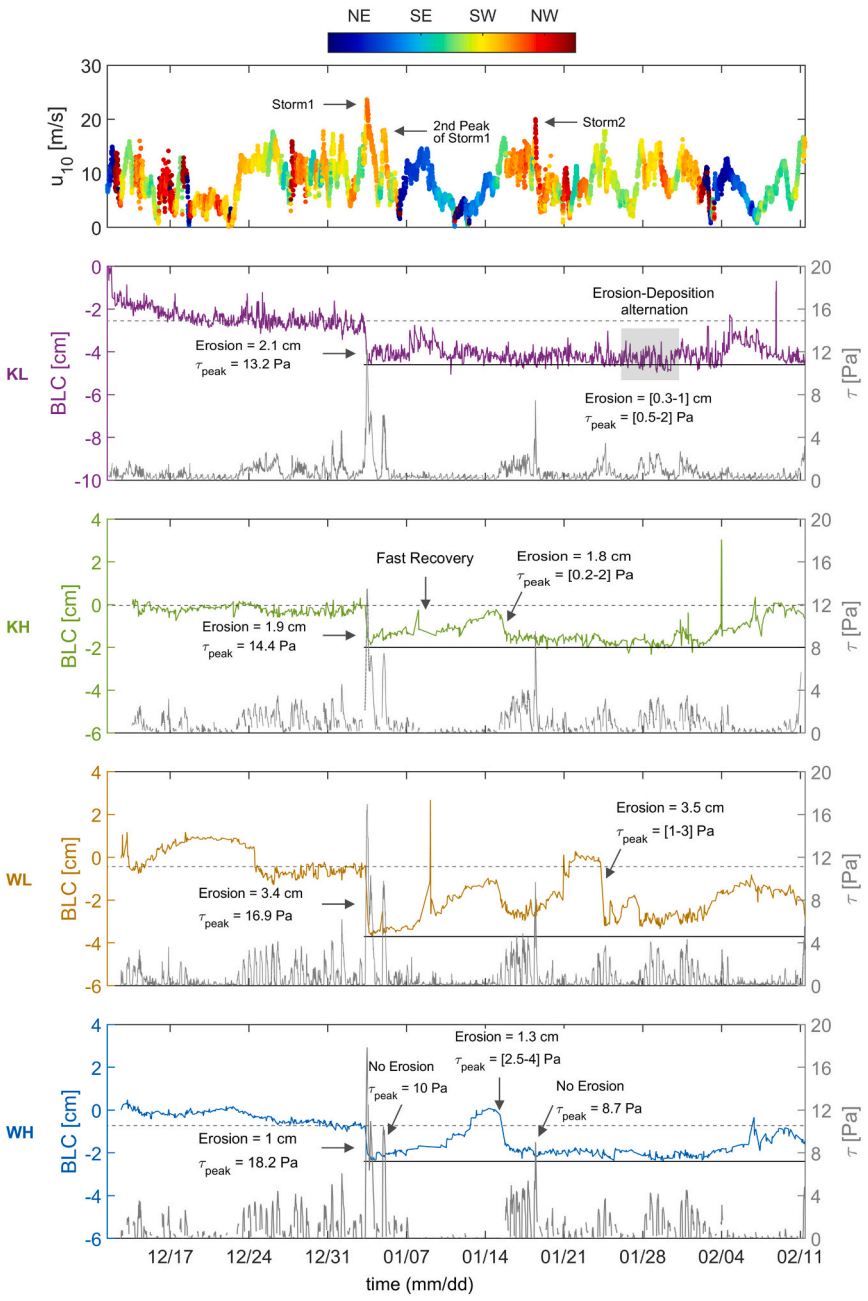

Fig. 4. Time series of wind, bed level changes (left-axes) and maximum wave-current bed shear stress (right-axes) during the winter measurement period. The dashed vertical lines indicate the moment of the first and second storms (January 3 and 16, respectively).

SSC at the turbid fringe) does not occur during conditions with the largest wave-induced orbital motions, but during the period with the highest flow velocities, occurring at the beginning of the flood phase. This is in contrast with the suggestion in Green (2003), where the waves are identified as most important.

3.3.2. *Deposition of fluid mud*

One event resulted in 16 cm sediment deposition at site WH (Fig. 8). This sedimentation event directly followed the January 3–5 storm ('Storm1' in Fig. 4), which induced on average 3 cm erosion of the mudflats. Wind conditions in the post-storm period (NE-SE wind) resulted in a set-down. As a consequence the bed remained completely emerged (or only briefly submerged) during several consecutive tidal cycles, especially at WH (Fig. 4). On January 8 the bed level at WL increased 4 cm in 1 h and 20 min (i.e. a deposition rate of 3 cm/h) during the flood phase, and was followed by stronger erosion during the ebb phase (5.5 cm in 50 min). The deposition and erosion rates at WH cannot be inferred from the dataset because the sensors were only shortly submerged. However, the peak in SSC up to 6 g/l and the relatively high flow velocity (0.3 m/s) suggests the passage of a highly concentrated suspension close to the bed. SSC are much lower during the two tidal cycles following the rapid deposition phase (3 g/l vs 6 g/l), and deposition is only 0.5 cm per tidal cycle.

Typically, the thickness of the deposited layer is larger at higher mudflat elevations: 3 cm at KL, 4 cm at WL, 4.2 cm at KH and 16 cm at WH. These relatively high deposition rates, accompanied by peaks in SSC, especially at higher mudflat elevations, suggest that these deposits are formed by fluid mud. Fluid mud deposits up to 20 cm thick have indeed been observed in the salt marshes fringing the mudflat of Westhoek (e.g. Baptist et al., 2019). However, our observations also show

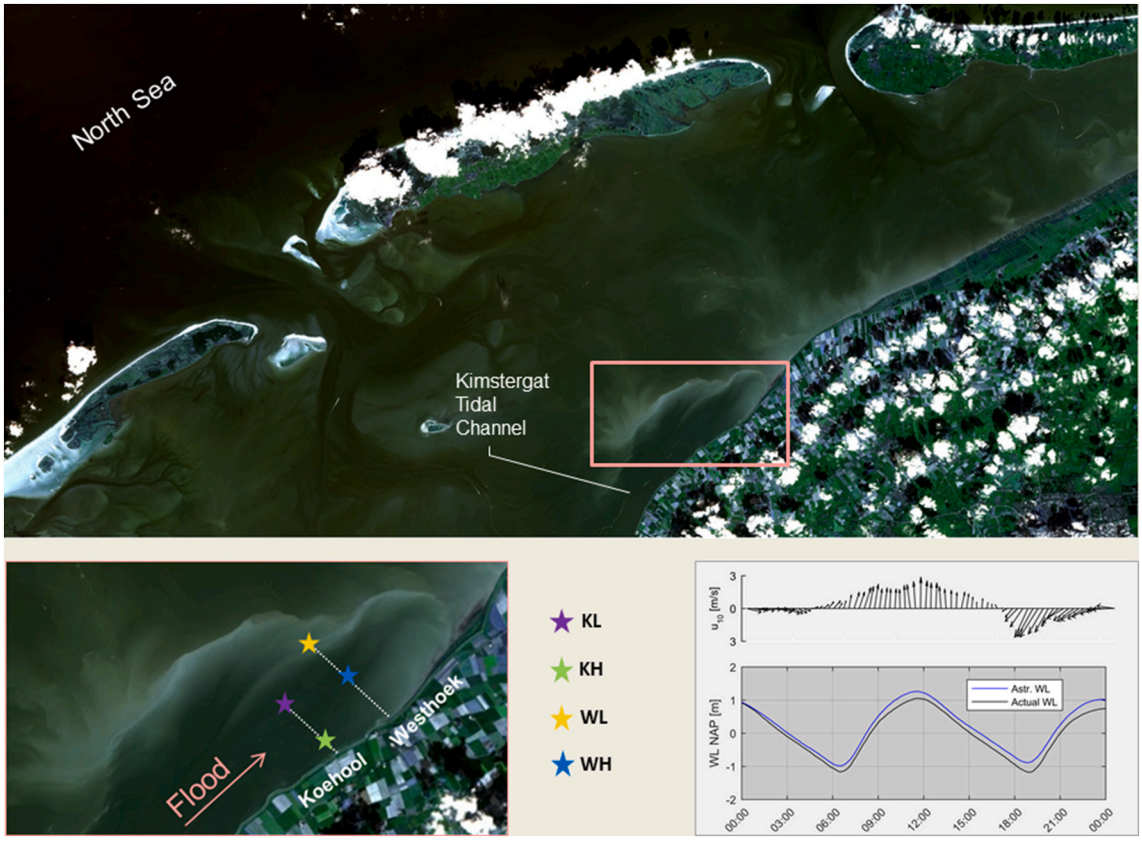

Fig. 5. Satellite picture of a turbid fringe on September 23, 2017 in our study site: overall view (top), detail (lower left) and water level and wind conditions on September 23, 2017 (lower right: wind below 3 m/s from the South and a water level set-down of about 20 cm.)

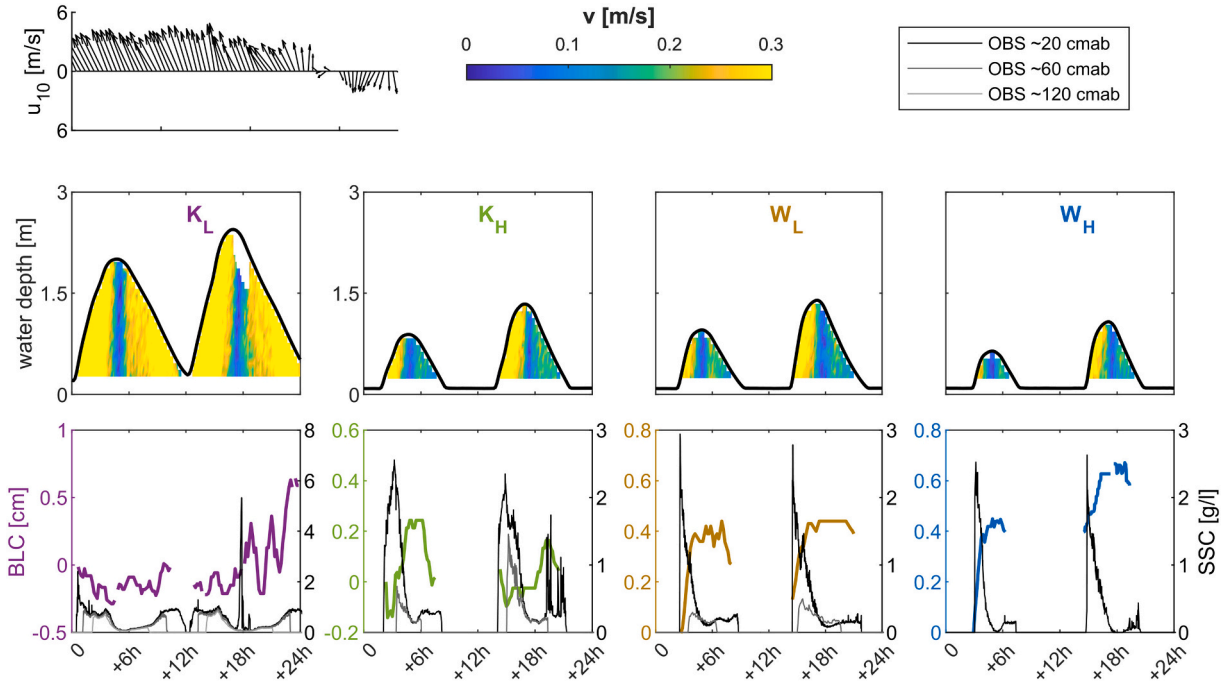

Fig. 6. SSC (at three heights) and flow velocity observed at the four measurement sites during the passage of a depositional turbid fringe on January 10, 2018. Wind conditions (top left panel) reveal that hydro-meteorological conditions are similar to those in Fig. 5.

that despite the rapid deposition rates, such fluid mud formation has very little impact on the bed levels over longer (days-weeks) time periods (Fig. 4). Its effect disappears within one tidal cycle (possibly also due to gravity, inducing a fluid mud transport towards the less elevated subtidal zones).

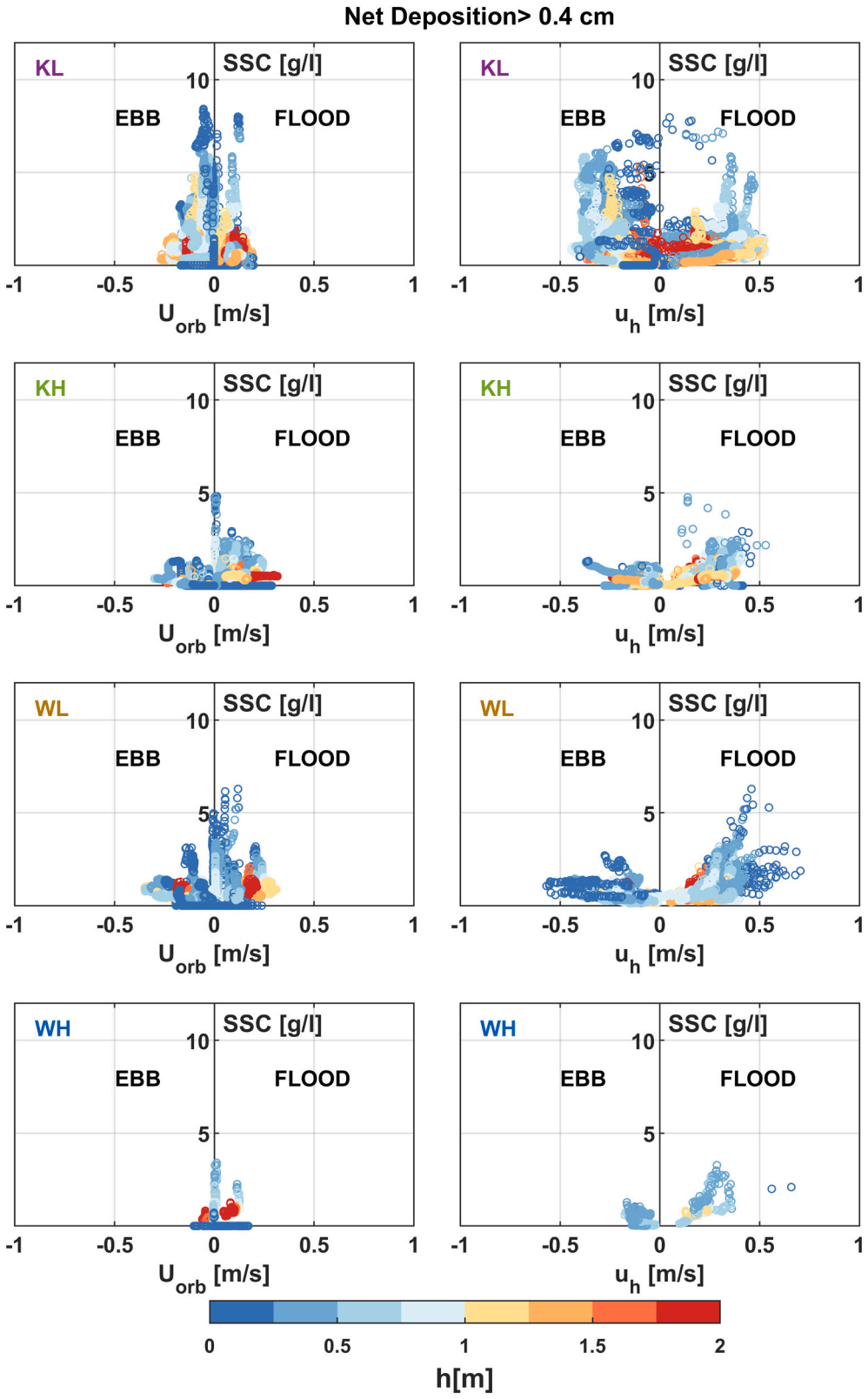

Fig. 7. SSC versus near-bed wave-orbital velocity (U_{orb}) and horizontal flow velocity at 20 cm above the bed (u_h) for tides with net deposition rates exceeding 0.4 cm (winter measurements). The colour of the markers provides the water depth.

3.4. Wind-induced effects on Inundation and consolidation

The morphodynamic development of tidal flats, as presented in the sections above, is strongly influenced by its inundation history (Reed, 1990; Friedrichs and Perry, 2001). A relatively long inundation duration implies more opportunity for sediment erosion and deposition, whereas a relatively short inundation duration results in longer air exposure, and therefore more opportunity for the sediment to over-consolidate.

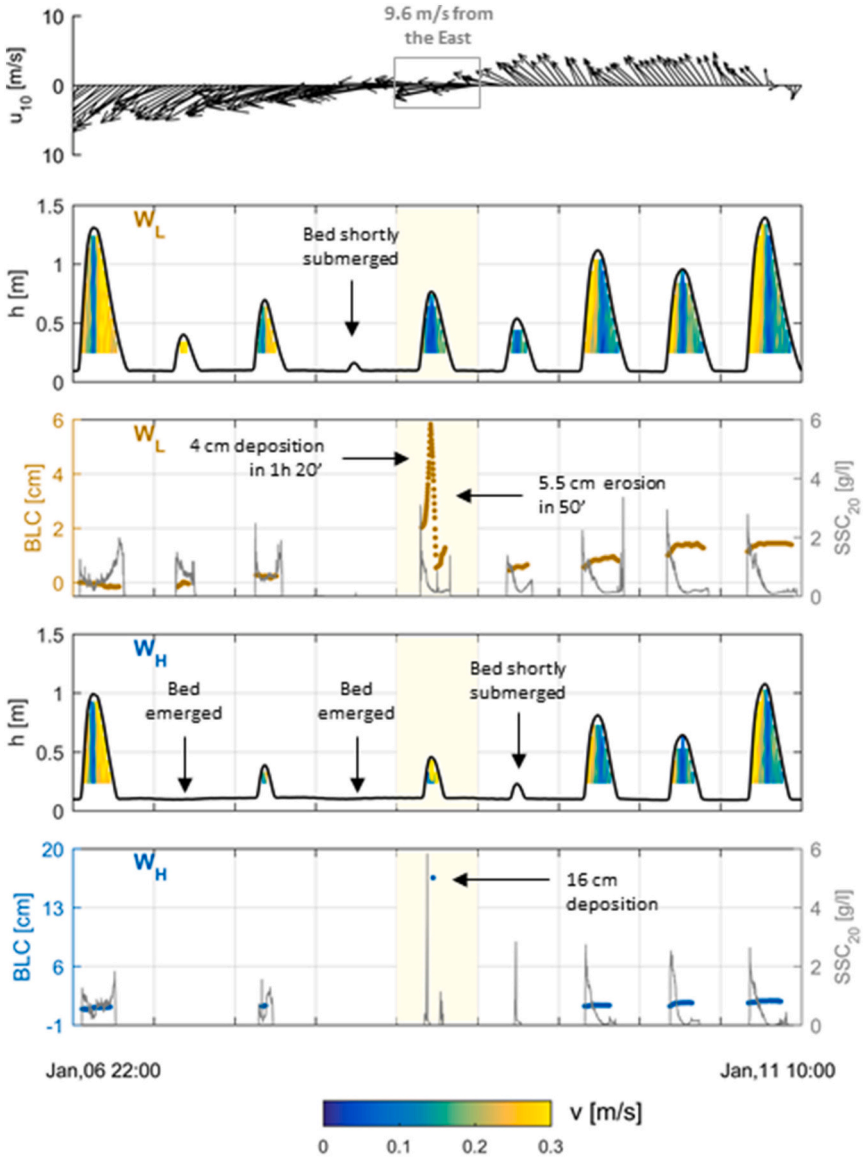

Fig. 8. Hydro-sedimentary conditions during a fluid formation event at station WL (panel 2 and 3) and WH (panel 4 and 5): water depth and flow velocity (panel 2, 4) and bed levels and SSC (panel 3, 5). Emerged conditions imply the absence of data.

Similarly, frequent inundation of the bed typically leads to a high water content of the muddy bed (and therefore less likely an over-consolidated state). Therefore, both the frequency and duration are important.

We evaluate the effect of wind on the inundation using 2-weeks of actual and astronomical water levels (Dec 31-Jan 14, i.e. winter field campaign). The inundation is governed by tides, but also by wind conditions (exemplified by eastern and western winds in Fig. 9). The inundation periods are longer in the period with wind-induced setup (Period 1), compared to the astronomical conditions. For these conditions the bed level at MHW (1.2 mMSL) is inundated for 18 % of time, and during 55 % of all tides. During a period of set-down (Period 2), the flooding duration and its recurrence decreases, with a maximum decrease of recurrence of 60 % at an elevation of 0.8 m. This sharp decrease in recurrence implies that a certain area of the tidal flat is emerged for several consecutive tidal cycles.

The emergence period is computed at five tidal flat elevations (ranging from Mean low Water (MLW = −1 mMSL) up to mean high Water (MHW = +1 mMSL)) and compared to wind conditions using 2 years of tidal and meteorological data (Fig. 10). The emergence duration is longer for wind blowing from the East and shortest for wind from the West. Especially for bed elevations higher than MSL, the emergence duration period becomes a multiple of the dominant tidal period. At BL = 0.5 mMSL the flat is typically emerged for either ~ 10 hours or ~ 22 hours because a small difference in water level may lead to a shift in the the exposure duration from one to two tidal cycles (see bottom panel in Fig. 10). Around MHW the emergence period may be as long as 334 h (14 days, corresponding to a spring-neap tidal cycle). These long periods of emergence are crucial for the long-term morphodynamic development because of consolidation processes that take place during periods of emergence.

3.5. *Impact of aerial exposure on consolidation*

The strength of aerially exposed tidal flat beds increase, and this change is generally attributed to evaporation processes (Fagherazzi et al., 2017; Nguyen et al., 2022). Our data shows how the wind influences the water level, flow velocities, sediment concentrations and bed level changes but do not cover in-situ bed shear strength development, as such measurements are extremely difficult in the field. Since strength development is important for understanding how tidal flat

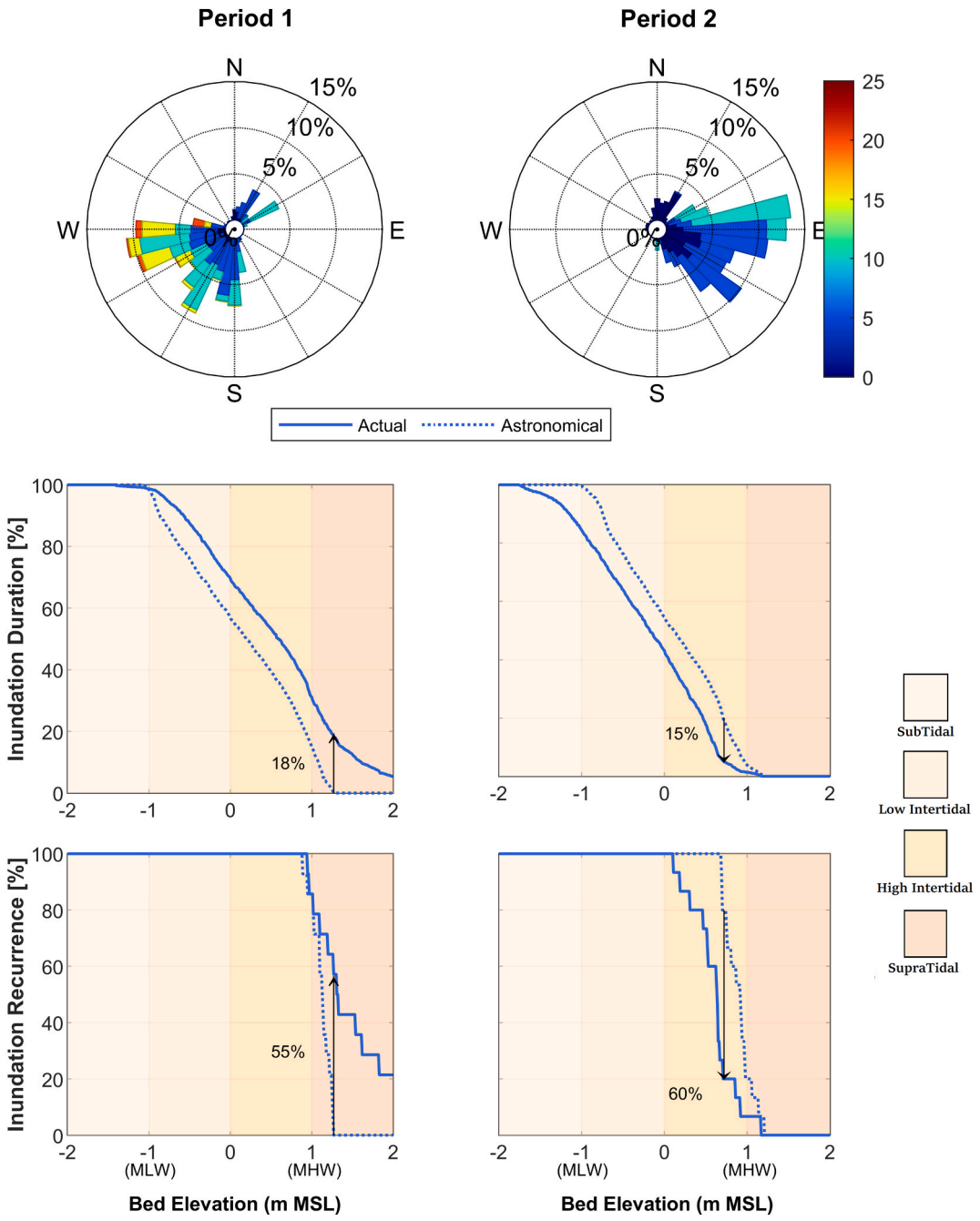

Fig. 9. Effect of the wind on inundation during Period 1 (left: Dec 31- January 6, strong (u_{10} >15 m/s) western winds, spring tide conditions) and Period 2 (right: January 7–14, moderate (u_{10} <10 m/s) eastern wind, neap tide conditions). The inundation frequency is defined as the percentage of time that a certain bed elevation is inundated at High Water Level (at Harlingen gauging station). The inundation duration is the percentage of time that a certain bed elevation is flooded.

dynamics respond to wind conditions, we elaborate on strength development here more conceptually.

The yield strength τ_y of the bed can be described by the fractal model of Kranenburg (1994):

$$\tau_y = K_y(\phi_s)^{\frac{2}{3-n_f}} \tag{1}$$

with sediment volume fraction ϕ_s, material parameter K_y and fractal dimension n_f. Since $n_f \approx 2.7$, the strength increases highly non-linear with the volume fraction: a small increase in sediment volume fraction can lead to a substantial increase in strength.

The sediment volume fraction of the bed ϕ_s can be described by Gibson's equation, which has the solution:

$$\frac{\phi_s(z) - \phi_{s,eq}}{\phi_{s,0} - \phi_{s,eq}} = \frac{z}{\sqrt{4\Gamma_{cons}t}} \tag{2}$$

where the subscripts '0' and 'eq' refer to the initial and equilibrium condition, Γ_{cons} [m^2/s] is the consolidation coefficient, and the vertical position z is defined as upwards positive.

The associated consolidation time for a mud layer, having thickness δ, is given by:

$$T_{cons} = \frac{\delta^2}{\Gamma_{cons}} \tag{3}$$

The consolidation coefficient Γ_{cons} is assumed constant (Winterwerp

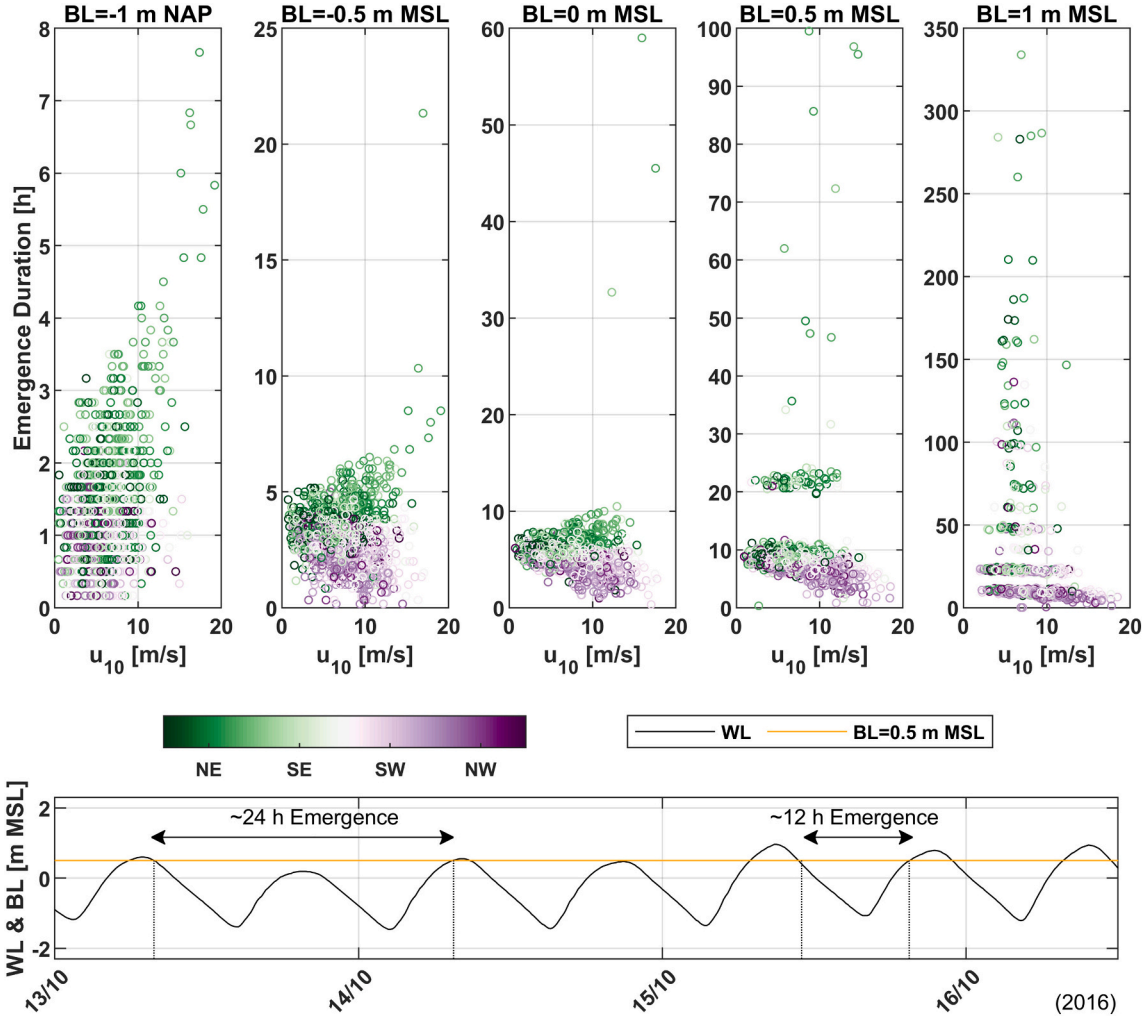

Fig. 10. Duration of tidal flat emergence at various tidal flat bed levels (BL) as a function of wind velocity u_{10} and direction (measured hourly in Leeuwarden) from January 2016 to December 2018. The emerged duration is determined using water levels (WL) measured every 10 min at Harlingen. Each dot corresponds to the time period in-between two consecutive inundations; it varies between 10 min (once per tidal cycle, short period of emergence) and multiple tidal cycles (long period of emergence), with wind direction playing a pivotal role. The mean wind speed and the dominant wind direction is computed by averaging meteorological data during the period of emergence. The water levels in the period 13 to 16 October 2016 (lower panel) explain why the emergence duration at bed elevations of 0.5 or 1.0 mMSL is often a multiple of ~12h: a small difference in MHW level doubles the emergence duration (the yellow line representing a bed level of 0.5 mMSL.) (For interpretation of the references to colour in this figure legend, the reader is referred to the web version of this article.)

et al., 2021), with $\Gamma_{cons} \simeq 10^{-8} - 10^{-7}$ m^2/s). The time scale is therefore strongly dependent on the thickness, with thick deposits having much longer consolidation times than thin layers. The equilibrium sediment volume fraction at position z depends on two contributions (Winterwerp et al., 2021): (1) the weight of the sediment above z, scaling with $Z_s - z$, with Z_s being the vertical position of the water-sediment interface and (2) the suction due to under pressures, scaling with the suction head $Z_s - Z_{ph}$ (the vertical distance between the water-sediment interface Z_s and the phreatic level Z_{ph}), resulting in:

$$\phi_{s,e}(z) = \left[\frac{n-1}{n}\frac{(\rho_s-\rho_w)g}{K_p}(Z_s - z) + \left(\frac{\rho_w g(Z_s - Z_{ph})}{K_p}\right)^{\frac{n-1}{n}}\right]^{\frac{1}{n-1}} \quad (4)$$

in which $n = 2/(3-n_f)$. A low phreatic level therefore increases consolidation rates, especially in the upper part of the bed, where $(Z_s - z) \ll (Z_s - Z_{ph})$, leading to over-consolidation. The consolidation rates resulting from underpressures are much larger than self-weight consolidation (the first term in Eq. (4)) due to the small thickness of the sediment deposits.

Next to the capillary suction from the lower phreatic level, evaporation increases the underpressures in the upper part of the bed further - see also Fagherazzi et al. (2017) and Nguyen et al. (2022). Longer emergence of a tidal flat leads to more evaporation and therefore larger underpressures. The sediment volume fraction will therefore increase with longer emergence and aerial exposure. Because of the non-linear relation between the sediment volume fraction and bed strength, a small increase in aerial exposure (and thus the sediment volume fraction) leads to a substantial increase in strength.

A straightforward example demonstrating the lack of opportunity for consolidation of thick deposited layers of fine sediment is fluid mud formation (Section 3.3.2, Fig. 8). Layers of several centimeters (4 to 16 cm) thick deposit over time frames of a few hours, during calm conditions following a storm. However, the deposited material is already eroded within the same tidal cycle because the material is very soft and easily erodible. Developing strength for this material to permanently deposit would require a very long period of low-energy or emerged conditions. Similarly, turbid fringes (analyzed in Section 3.3) resulting in a relatively rapid (timescales of hours) bed level increases (order of 0.5–1 cm) are effective for a long-term bed level accretion only if followed by relatively long air-exposure (i.e, wind direction inducing set-down is needed).

4. Discussion: windows of opportunity for tidal flat accretion

We identified four key interaction types between the wind and morphodynamics of tidal flats: (i) generation of waves and subsequent resuspension; (ii) generation of wind-driven flow leading to horizontal transport of sediment; (iii) water level set-up, leading to inundation, enabling sediment deposition; (iv) waterlevel set-down, increasing the aerial exposure period, stimulating over-consolidation of previously deposited sediments. The first two interaction types are well identified in previous studies. The role of wind on resuspension of fine sediments through generation of waves has been revealed by publications, see e.g. Allen and Duffy (1998); Ridderinkhof et al. (2000); Janssen-Stelder (2000); Yang et al. (2003b); Shi et al. (2015, 2017b); Zhu et al. (2016); Xie et al. (2018). The importance of wind-driven flow on sediment transport in general is also well established (Baeye et al., 2011; Xie et al., 2018; De Vet et al., 2018; Yang et al., 2023b). In the Wadden Sea an eastward directed transport component exists, resulting from wind through both the larger channels (Nauw et al., 2014; Duran-Matute et al., 2014, 2016; Sassi et al., 2015, 2016)) and over flats Colosimo et al. (2020); van Weerdenburg et al. (2021). However, the importance of interaction types (iii) and (iv) are new, especially in combination with (i) and (ii).

As the wind varies both in speed and direction, various sequences of these four interaction types may occur. Based on extensive field experiments presented here, we argue that tidal flat accretion is only possible if: (1) there is a period with sufficient deposition and (2) this period is followed by a period in which the bed can (over) consolidate, thereby developing sufficient strength to withstand the following erosion event. The wind therefore drives the physical processes (resuspension, deposition, consolidation) controlling net accretion. In an analogue to a window of opportunity, we refer to this sequence of events as the'Winds of Opportunity'. For our measurement location, a period with weak to moderate wind from the southwest can lead to deposition. In order to lead to permanent accretion, this deposition phase should be followed by a period with moderate wind from the southeast to induce water level set-down.

Projecting the concept of these winds of opportunity to a tidal flat, it is expected that the sequential order of deposition, consolidation and erosion cross-sectionally varies as schematized in Fig. 11. On the lower flat the cumulative changes in bed elevation are larger than on the higher flat (Fig. 2): a larger submergence duration implies a larger window for deposition. However, due to the short aerial exposure period, over-consolidation and therefore strength development is limited. A relatively small storm will already lead to erosion of the freshly deposited sediments and therefore large deposition rates do not necessarily lead to large accretion rates.

The window for consolidation is larger on the higher flat than on the lower flat for several reasons. Most importantly, the area is exposed longer by tidal action and by variability introduced by the wind (Fig. 9), leading to (over) consolidation. Secondly, the sediment concentration (and therefore the deposition rate) is lower on the upper flat. Fig. 7, for instance, shows that the occurrence of large sediment deposition (net bed level change $>$ 0.4 cm) relates to the occurrence of 'depositional' turbid fringes. The maximum SSC measured during the passage of such a turbid fringe decreases at higher bed elevations (Fig. 7) in concert with a decrease of flow velocity (Fig. 6). Lower SSC results in thinner bed deposits which consolidate more rapidly. Both aspects result in a relatively uniform bed response to winter storms (erosion everywhere) but spatially varying post-storm recovery (Fig. 4). The bed of the lower flat did not recover from the storm-induced erosion, whereas at the higher elevations an almost full recovery occurred within the two weeks following the event.

Our conceptual model can also (partly) explain the development of bed stratigraphy and cliffs in fine-grained tidal environments. The development of bed stratigraphy is typically associated with a textural variability reflecting its depositional environment, which in turn determines the erodibility (van Rijn, 2020; Mitchener and Torfs, 1996; Van Ledden et al., 2004). In fine-grained environments the bed stratigraphy is often in the form of very fine laminations (e.g. see a photograph taken at Westhoek in Fig. 12), and we hypothesize that such layering may reflect historic phases in overconsolidation rather than a difference in grain size.

The horizontal gradients in sediment deposition and consolidation may give rise to cliff formation. Cliff erosion is caused by mass erosion, induced by waves. As the bed is over-consolidated,"normal" stresses cannot erode the bed (surface erosion). In case evaporation is the dominant over-consolidation agent, the bed is stronger at its surface than at greater depth. The wave-induced stresses are also larger a bit further down within the sediment bed, which explains the erosion of lumps of material (Winterwerp et al., 2012). As discussed, the degree of over-consolidation generally increases up-flat. The inundated tidal flat may therefore erode relatively easily and gradually, whereas the higher flat gains strength and is only eroded as mass erosion. This leads to cliff formation at the transition zone from under-consolidated to over-consolidated sediment beds.

A crucial question then arises whether bed level accretion is limited

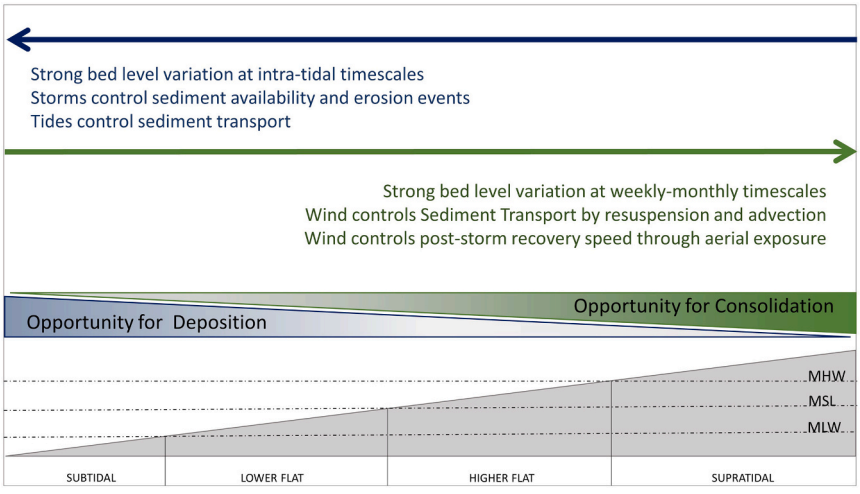

Fig. 11. The relative importance of the processes controlling tidal flat accretion across a tidal flat, with a strong tidal influence and regular opportunities for deposition over the lower flat and a strong wind-driven influence and opportunities for consolidation over the upper flat. Net accretion requires a temporal sequence of consolidation following deposition.

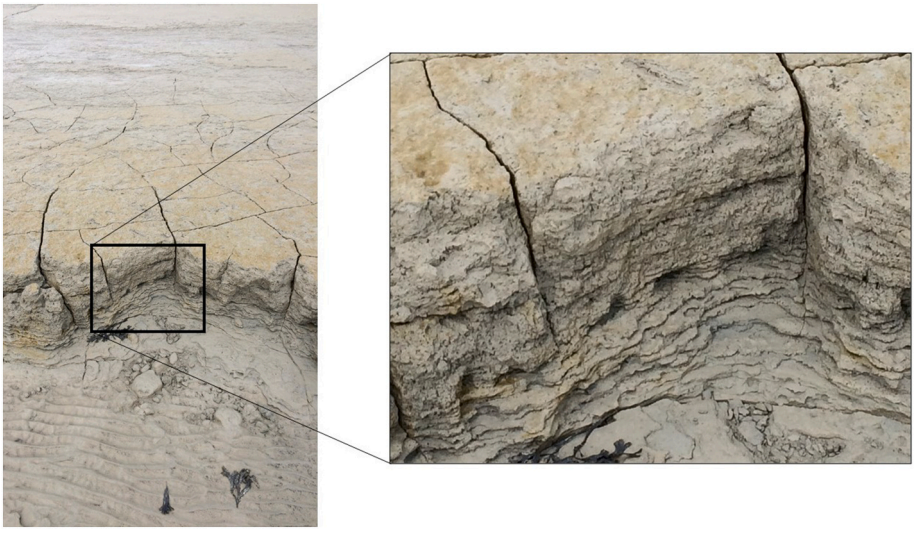

Fig. 12. Cliff developed in the upper intertdal zone at Westhoek, revealing fine laminations of mud-dominated deposit.

by sediment deposition rates or consolidation rates. For Westhoek and Koehool, periods of deposition led to a bed level increase of centimeters per week. This suggests that there is sufficient sediment available and that the sediment is able to deposit. However, erosion events lead to erosion of the freshly deposited sediment. This indicates that over-consolidation is likely the limiting factor for tidal flat accretion. During summer conditions, with generally lower sediment concentrations and less storm setup, deposition rates may become a limiting factor. The limiting factor also varies over the tidal flat profile. Higher parts of the flats (not monitored as part of our surveys) and especially over the supratidal salt marshes, deposition events become progressively more important for accretion. Summarizing, net accretion rates are controlled by (over-)consolidation rates in winter (sediment deposition rates are sufficient) and by deposition rates in summer (especially on the upper flat, where consolidation rates are high).

5. Conclusions

The present study analyzes the processes contributing to the vertical accretion of a tidal flat bed in a fine-grained sediment environment and identifies a window of opportunity for fine sediment accretion over long timescales. This window of opportunity reflects a temporal sequence of sediment deposition and sediment consolidation, resulting in the formation of a new layer of over-consolidated sediment.

Sediment may deposit for several tidal cycles during conditions with relatively large supply and mild hydrodynamic conditions. However, on longer time scales (weeks-months) the combined wave-current forcing easily erodes this relatively fresh material. This implies that although sediment may deposit it does not gain sufficient strength to withstand even minor wave-induced resuspension events. Therefore, erosion resulting from relatively strong storms has a long-lasting effect (months to years). Recovery from such a storm-induced setback is not only dependant on the opportunity for deposition (as abundant sediment is typically available after storms) but especially on the opportunity for consolidation. Crucial hereby is that the strength of the bed resulting from self-weight consolidation is too weak (and requires a very long time) to withstand erosion during subsequent storm conditions; sufficient strength is only attained through over-consolidation resulting from a low water table, evaporation and drying.

Conditions favoring over-consolidation are largely driven by the wind. Winds therefore not only affect the morphological evolution of the mudflats by regulating the bed shear stress, but also by creating favourable conditions for sediment over-consolidation. Winds inducing water level set-down (at our study site, eastern wind) contribute to the reduction of inundation duration and of inundation frequency, favoring aerial exposure of the mudflat and therefore, the over-consolidation process and strength development.

Our study also shows that long-term vertical accretion of tidal flats may even be limited in case of large sediment availability because the resulting mud deposits are too thick to rapidly consolidate and develop strength. As a result, the sediments are continuously deposited and eroded, while net mudflat accretion rates remains small.

Declaration of competing interest

The authors declare that they have no known competing financial interests or personal relationships that could have appeared to influence the work reported in this paper.

Data availability

Data will be made available on request.

Acknowledgements

This study is part of the research program Sediment for Salt Marshes: Physical and Ecological Aspects of a Mud Motor with project number 13888, which is financed by The Netherlands Organization for Scientific Research (NWO). DSM received funding from the Programme of Strategic Scientific Alliances between China and the Netherlands and the Zijiang Scholar Program of East China Normal University.

References

Allen, J., Duffy, M., 1998. Medium-term sedimentation on high intertidal mudflats and salt marshes in the Severn estuary, sw britain: the role of wind and tide. Mar. Geol. 150 (1–4), 1–27.

Andersen, T., Pejrup .3., M., 2001. Suspended sediment transport on a temperate, microtidal mudflat, the Danish Wadden Sea. Mar. Geol. 173 (1–4), 69–85. https://linkinghub.elsevier.com/retrieve/pii/S002532270000164X.

Andersen, T.J., Pejrup, M., Nielsen, A.A., 2006. Long-term and high-resolution measurements of bed level changes in a temperate, microtidal coastal lagoon. Mar. Geol. 226 (1–2), 115–125.

Baeye, M., Fettweis, M., Voulgaris, G., Van Lancker, V., 2011. Sediment mobility in response to tidal and wind-driven flows along the Belgian inner shelf, southern North Sea. Ocean Dyn. 61 (5), 611–622.

Baptist, M.J., Gerkema, T., van Prooijen, B.C., van Maren, D.S., van Regteren, M., Schulz, K., Colosimo, I., Vroom, J., van Kessel, T., Grasmeijer, B., Willemsen, P., Elschot, K., de Groot, A.V., Cleveringa, J., van Eekelen, E.M., Schuurman, F., de Lange, H.J., van Puijenbroek, M.E., 2019. Beneficial use of dredged sediment to enhance salt marsh development by applying a 'Mud Motor'. Ecol. Eng. 127 (December 2018), 312–323. https://doi.org/10.1016/j.ecoleng.2018.11.019.

Barbier, E.B., Hacker, S.D., Kennedy, C., Kock, E.W., Stier, A.C., Sillman, B.R., 2011. The value of estuarine and coastal ecosystem services. Ecol. Monogr. 81 (2), 169–193.
Bassoullet, P., Le Hir, P., Gouleau, D., Robert, S., 2000. Sediment transport over an intertidal mudflat: Field investigations and estimation of fluxes within the 'Baie de Marennes-Oleron' (France). Cont. Shelf Res. 20 (12–13), 1635–1653.
Been, K., Sills, G., 1981. Self-weight consolidation of soft soils: an experimental and theoretical study. Geotechnique 31 (4), 519–535.
Belliard, J.P., Silinski, A., Meire, D., Kolokythas, G., Levy, Y., Van Braeckel, A., Bouma, T. J., Temmerman, S., 2019. High-resolution bed level changes in relation to tidal and wave forcing on a narrow fringing macrotidal flat: Bridging intra-tidal, daily and seasonal sediment dynamics. Mar. Geol. 412, 123–138.
Bundgaard, K., Lumborg, U., 2019. Challenges in using optical backscatter techniques for sediment monitoring in mixed sediment environments. Terra et Aqua 154, 22–29.
Colina Alonso, A., van Maren, D.S., Elias, E.P., Holthuijsen, S.J., Wang, Z.B., 2021. The contribution of sand and mud to infilling of tidal basins in response to a closure dam. Mar. Geol. 439 (February), 106544 https://doi.org/10.1016/j.margeo.2021.106544.
Colosimo, I., de Vet, P.L.M., van Maren, D.S., Reniers, A.J.H.M., Winterwerp, J.C., van Prooijen, B.C., 2020. The impact of wind on flow and sediment transport over intertidal flats. J. Mar. Sci. Eng. 8 (11), 910. https://www.mdpi.com/2077-1312/8/11/910.
De Vet, P.L.M., van Prooijen, B.C., Schrijvershof, R.A., van der Werf, J.J., Ysebaert, T., Schrijver, M.C., Wang, Z.B., 2018. The importance of combined tidal and meteorological forces for the flow and sediment transport on intertidal shoals. J. Geophys. Res. Earth Surf. 123 (10), 2464–2480. https://doi.org/10.1029/2018JF004605.
Deloffre, J., Verney, R., Lafite, R., Lesueur, P., Lesourd, S., Cundy, A., 2007. Sedimentation on intertidal mudflats in the lower part of macrotidal estuaries: sedimentation rhythms and their preservation. Mar. Geol. 241 (1–4), 19–32. https://linkinghub.elsevier.com/retrieve/pii/S0025322707000618.
Dethier, E.N., Renshaw, C.E., Magilligan, F.J., 2022. Rapid changes to global river suspended sediment flux by humans. Science 376 (6600), 1447–1452.
Downing, J., 2006. Twenty-five years with OBS sensors: the good, the bad, and the ugly. Cont. Shelf Res. 26 (17–18), 2299–2318. https://linkinghub.elsevier.com/retrieve/pii/S0278434306002469.
Duran-Matute, M., Gerkema, T., De Boer, G.J., Nauw, J.J., Gräwe, U., 2014. Residual circulation and freshwater transport in the Dutch Wadden Sea: a numerical modelling study. Ocean Sci. 10 (4), 611–632.
Duran-Matute, M., Gerkema, T., Sassi, M.G., 2016. Quantifying the residual volume transport through a multiple-inlet system in response to wind forcing: the case of the western d utch w adden s ea. J. Geophys. Res. Oceans 121 (12), 8888–8903.
Elias, E.P., Van Der Spek, A.J., Wang, Z.B., De Ronde, J., 2012. Morphodynamic development and sediment budget of the Dutch Wadden Sea over the last century. Geologie en Mijnbouw Netherlands J. Geosci. 91 (3), 293–310.
Elias, E.P., Van der Spek, A.J., Pearson, S.G., Cleveringa, J., 2019. Understanding sediment bypassing processes through analysis of high-frequency observations of ameland inlet, the Netherlands. Mar. Geol. 415, 105956. https://www.sciencedirect.com/science/article/pii/S0025322718304997.
Fagherazzi, S., Viggato, T., Vieillard, A., Mariotti, G., Fulweiler, R., 2017. The effect of evaporation on the erodibility of mudflats in a mesotidal estuary. Estuar. Coast. Shelf Sci. 194, 118–127.
Fan, D., Li, C., 2002. Rhythmic deposition on mudflats in the mesotidal changjiang estuary, China. J. Sediment. Res. 72 (4), 543–551.
Fan, D., Li, C., Archer, A.W., Wang, P., 2002. Temporal distribution of diastems in deposits of an open-coast tidal flat with high suspended sediment concentrations. Sediment. Geol. 152 (3–4), 173–181.
Fan, D., Guo, Y., Wang, P., Shi, J.Z., 2006. Cross-shore variations in morphodynamic processes of an open-coast mudflat in the changjiang delta, China: with an emphasis on storm impacts. Cont. Shelf Res. 26 (4), 517–538.
Friedrichs, C.T., Perry, J.E., 2001. Tidal Salt Marsh Morphodynamics: a Synthesis. J. Coast. Res. 27, 7–37. http://www.jstor.org/stable/25736162.
Garwood, J.C., Hill, P.S., MacIntyre, H.L., Law, B.A., 2015. Grain sizes retained by diatom biofilms during erosion on tidal flats linked to bed sediment texture. Cont. Shelf Res. 104, 37–44.
Gerkema, T., Nauw, J., van der Hout, C., 2014. Measurements on the transport of suspended particulate matter in the Vlie Inlet. Netherlands J. Geosci. Geologie en Mijnbouw 93 (3), 95–105. https://www.cambridge.org/core/product/identifier/S0016774614000079/type/journal_article.
Goring, D.G., Nikora, V.I., 2002. Despiking acoustic Doppler velocimeter data. J. Hydraul. Eng. 128 (1), 117–126. https://doi.org/10.1061/%28ASCE%290733-9429%282002%29128%3A1%28117%29.
Green, M., 2003. The dance of the turbid fringe. Water Atmos. 11 (2), 20–21.
Green, M.O., Bell, R.G., Dolphin, T.J., Swales, A., 2000. Silt and sand transport in a deep tidal channel of a large estuary (Manukau Harbour, New Zealand). Mar. Geol. 163 (1–4), 217–240. https://linkinghub.elsevier.com/retrieve/pii/S0025322799001024.
Hache, I., Karius, V., Gutkuhn, J., von Eynatten, H., 2019. The development and application of an autonomous working turbidity measurement network: assessing the spatial and temporal distribution of suspended particulate matter on tidal flats in the north frisian wadden sea. Cont. Shelf Res. 176, 36–50. https://www.sciencedirect.com/science/article/pii/S0278434318304229.
Hir, P.L., Roberts, W., Cazaillet, O., Christie, M., Bassoullet, P., Bacher, C., 2000. Characterization of intertidal # at hydrodynamics. Cont. Shelf Res. 20, 1433–1459.
Hoitink, A., Hoekstra, P., 2005. Observations of suspended sediment from adcp and obs measurements in a mud-dominated environment. Coast. Eng. 52 (2), 103–118. https://www.sciencedirect.com/science/article/pii/S0378383904001346.
van der Hout, C.M., Gerkema, T., Nauw, J.J., Ridderinkhof, H., 2015. Observations of a narrow zone of high suspended particulate matter (spm) concentrations along the dutch coast. Cont. Shelf Res. 95, 27–38. https://www.sciencedirect.com/science/article/pii/S0278434315000126.
Janssen-Stelder, B., 2000. The effect of different hydrodynamic conditions on the morphodynamics of a tidal mudflat in the dutch wadden sea. Cont. Shelf Res. 20 (12–13), 1461–1478.
Kirwan, M.L., Megonigal, J.P., 2013. Tidal wetland stability in the face of human impacts and sea-level rise. Nature 504 (7478), 53–60.
Kirwan, M.L., Temmerman, S., Skeehan, E.E., Guntenspergen, G.R., Fagherazzi, S., 2016. Overestimation of Marsh Vulnerability to Sea Level Rise.
Kornman, B.A., Deckere, E.M.D., 1998. Temporal variation in sediment erodibility and suspended sediment dynamics in the dollard estuary. Geol. Soc. Lond., Spec. Publ. 139 (1), 231–241.
Kranenburg, C., 1994. The fractal structure of cohesive sediment aggregates. Estuar. Coast. Shelf Sci. 39 (5), 451–460.
Le Hir, P., Monbet, Y., Orvain, F., 2007. Sediment erodability in sediment transport modelling: can we account for biota effects? Cont. Shelf Res. 27 (8), 1116–1142.
Le Hir, P., Cayocca, F., Waeles, B., 2011. Dynamics of sand and mud mixtures: a multiprocess-based modelling strategy. Cont. Shelf Res. 31 (10), S135–S149.
Li, Y., Li, H., Qiao, L., Xu, Y., Yin, X., He, J., 2015. Storm deposition layer on the Fujian coast generated by typhoon saola (2012). Sci. Rep. 5 (1), 14904.
Li, L., Ni, J., Chang, F., Yue, Y., Frolova, N., Magritsky, D., Borthwick, A.G., Ciais, P., Wang, Y., Zheng, C., et al., 2020. Global trends in water and sediment fluxes of the world's large rivers. Sci. Bull. 65 (1), 62–69.
Malarkey, J., Baas, J.H., Hope, J.A., Aspden, R.J., Parsons, D.R., Peakall, J., Paterson, D. M., Schindler, R.J., Ye, L., Lichtman, I.D., et al., 2015. The pervasive role of biological cohesion in bedform development. Nat. Commun. 6 (1), 6257.
Merckelbach, L., Kranenburg, C., 2004. Equations for effective stress and permeability of soft mud–sand mixtures. Géotechnique 54 (4), 235–243.
Mitchener, H., Torfs, H., 1996. Erosion of mud/sand mixtures. Coast. Eng. 29 (1–2), 1–25.
Möller, I., Kudella, M., Rupprecht, F., Spencer, T., Paul, M., Van Wesenbeeck, B.K., Wolters, G., Jensen, K., Bouma, T.J., Miranda-Lange, M., et al., 2014. Wave attenuation over coastal salt marshes under storm surge conditions. Nat. Geosci. 7 (10), 727–731.
Nauw, J., Merckelbach, L., Ridderinkhof, H., Van Aken, H., 2014. Long-term ferry-based observations of the suspended sediment fluxes through the marsdiep inlet using acoustic doppler current profilers. J. Sea Res. 87, 17–29.
Nguyen, H.M., Bryan, K.R., Zhou, Z., Pilditch, C.A., 2022. Modeling the effects of aerial temperature and exposure period on intertidal mudflat profiles. Cont. Shelf Res. 245, 104802.
Orvain, F., Le Hir, P., Sauriau, P.-G., Lefebvre, S., 2012. Modelling the effects of macrofauna on sediment transport and bed elevation: Application over a cross-shore mudflat profile and model validation. Estuar. Coast. Shelf Sci. 108, 64–75.
Parsons, D.R., Schindler, R.J., Hope, J.A., Malarkey, J., Baas, J.H., Peakall, J., Manning, A.J., Ye, L., Simmons, S., Paterson, D.M., et al., 2016. The role of biophysical cohesion on subaqueous bed form size. Geophys. Res. Lett. 43 (4), 1566–1573.
Paterson, D., Hagerthey, S., 2001. Microphytobenthos in constrasting coastal ecosystems: biology and dynamics. Ecol. Compar. Sediment. Shores 105–125.
Pearson, S.G., Verney, R., van Prooijen, B.C., Tran, D., Hendriks, E.C.M., Jacquet, M., Wang, Z.B., 2021. Characterizing the composition of sand and mud suspensions in coastal and estuarine environments using combined optical and acoustic measurements. J. Geophys. Res. Oceans 126 (7). https://doi.org/10.1029/2021JC017354 (e2021JC017354, e2021JC017354 2021JC017354).
van Prooijen, B.C., Tissier, M.F.S., de Wit, F.P., Pearson, S.G., Brakenhoff, L.B., van Maarseveen, M.C.G., van der Vegt, M., Mol, J.-W., Kok, F., Holzhauer, H., van der Werf, J.J., Vermaas, T., Gawehn, M., Grasmeijer, B., Elias, E.P.L., Tonnon, P.K., Santinelli, G., Antolnez, J.A.A., de Vet, P.L.M., Reniers, A.J.H.M., Wang, Z.B., den Heijer, C., van Gelder-Maas, C., Wilmink, R.J.A., Schipper, C.A., de Looff, H., 2020. Measurements of hydrodynamics, sediment, morphology and benthos on ameland ebb-tidal delta and lower shoreface. Earth Syst. Sci. Data 12 (4), 2775–2786. https://essd.copernicus.org/articles/12/2775/2020/.
Reed, D., 1990. The impact of sea-level rise marshes. Prog. Phys. Geogr. 14 (4), 465–481.
Reed, D.J., 1995. The response of coastal marshes to sealevel rise: survival or submergence? Earth Surf. Process 20, 39–48.
Ridderinkhof, H., van der Ham, R., van der Lee, W., 2000. Temporal variations in concentration and transport of suspended sediments in a channel–flat system in the ems-dollard estuary. Cont. Shelf Res. 20 (12–13), 1479–1493.
Riedel, T., Lettmann, K., Beck, M., Brumsack, H.-J., 2010. Tidal variations in groundwater storage and associated discharge from an intertidal coastal aquifer. J. Geophys. Res. Oceans 115 (C4).
van Rijn, L.C., 2020. Erodibility of mud–sand bed mixtures. J. Hydraul. Eng. 146 (1), 04019050.
van Rijn, L.C., Barth, R., 2019. Settling and consolidation of soft mud–sand layers. J. Waterw. Port Coast. Ocean Eng. 145 (1), 04018028.
Sanford, L.P., 2008. Modeling a dynamically varying mixed sediment bed with erosion, deposition, bioturbation, consolidation, and armoring. Comput. Geosci. 34 (10), 1263–1283.
Sassi, M., Duran-Matute, M., van Kessel, T., Gerkema, T., 2015. Variability of residual fluxes of suspended sediment in a multiple tidal-inlet system: the Dutch Wadden Sea. Ocean Dyn. 65 (9–10), 1321–1333. https://doi.org/10.1007/s10236-015-0866-2.
Sassi, M.G., Gerkema, T., Duran-Matute, M., Nauw, J.J., 2016. Residual water transport in the marsdiep tidal inlet inferred from observations and a numerical model. J. Mar. Res. 74 (1), 21–42.

Shi, B., Yang, S., Wang, Y., Bouma, T., Zhu, Q., 2012. Relating accretion and erosion at an exposed tidal wetland to the bottom shear stress of combined current–wave action. Geomorphology 138 (1), 380–389.
Shi, B., Wang, Y.P., Yang, Y., Li, M., Li, P., Ni, W., Gao, J., 2015. Determination of critical shear stresses for erosion and deposition based on in situ measurements of currents and waves over an intertidal mudflat. J. Coast. Res. 31 (6), 1344–1356.
Shi, B., Cooper, J.R., Pratolongo, P.D., Gao, S., Bouma, T.J., Li, G., Li, C., Yang, S.L., Wang, Y.P., 2017a. a. erosion and accretion on a mudflat: the importance of very shallow-water effects. J. Geophys. Res. Oceans 122 (12), 9476–9499.
Shi, B., Yang, S., Wang, Y., Li, G., Li, M., Li, P., Li, C., 2017b. Role of wind in erosion-accretion cycles on an estuarine mudflat. J. Geophys. Res. Oceans 122 (1), 193–206.
Soulsby, R., 1995. Bed shear-stresses due to combined waves and currents. Adv. Coast. Morphodyn. 20–23. http://ci.nii.ac.jp/naid/10016530280/en/.
Syvitski, J.P.M., Vorosmarty, C.J., Kettner, A.J., Green, P., 2005. Impact of humans on the flux of terrestrial sediment to the global coastal ocean. science 308 (5720), 376–380.
Temmerman, S., Horstman, E.M., Krauss, K.W., Mullarney, J.C., Pelckmans, I., Schoutens, K., 2023. Marshes and mangroves as nature-based coastal storm buffers. Annu. Rev. Mar. Sci. 15, 95–118.
Timmerman, A., Haasnoot, M., Middelkoop, H., Bouma, T., McEvoy, S., 2021. Ecological consequences of sea level rise and flood protection strategies in shallow coastal systems: a quick-scan barcoding approach. Ocean Coast. Manag. 210, 105674. https://doi.org/10.1016/j.ocecoaman.2021.105674.
Torfs, H., Mitchener, H., Huysentruyt, H., Toorman, E., 1996. Settling and consolidation of mud/sand mixtures. Coast. Eng. 29 (1–2), 27–45.
Tucker, M., Pitt, E., 2001. Waves in Ocean Engineering. Elsevier, Amsterdam.
Turner, R.E., Baustian, J.J., Swenson, E.M., Spicer, J.S., 2006. Wetland sedimentation from hurricanes katrina and rita. Science 314 (5798), 449–452.
Van Ledden, M., Van Kesteren, W., Winterwerp, J., 2004. A conceptual framework for the erosion behaviour of sand–mud mixtures. Cont. Shelf Res. 24 (1), 1–11.
Van Maren, D.S., Colina Alonso, A., Engels, A., Vandenbruwaene, W., de Vet, P., Vroom, J., Wang, Z., 2023. Adaptation timescales of estuarine systems to human interventions. Front. Earth Sci. 11.
Van Prooijen, B.C., Winterwerp, J.C., 2010. A stochastic formulation for erosion of cohesive sediments. J. Geophys. Res. 115 (C1), C01005. https://doi.org/10.1029/2008JC005189.
de Vet, P.L., van Prooijen, B.C., Colosimo, I., Steiner, N., Ysebaert, T., Herman, P.M., Wang, Z.B., 2020. Variations in Storm-Induced Bed Level Dynamics across Intertidal Flats. Scientific Reports.
Vuik, V., Van Vuren, S., Borsje, B.W., van Wesenbeeck, B.K., Jonkman, S.N., 2018. Assessing safety of nature-based flood defenses: dealing with extremes and uncertainties. Coast. Eng. 139, 47–64.
van Weerdenburg, R., Pearson, S., van Prooijen, B., Laan, S., Elias, E., Tonnon, P.K., Wang, Z.B., 2021. Field measurements and numerical modelling of wind-driven exchange flows in a tidal inlet system in the dutch wadden sea. Ocean Coast. Manag. 215, 105941.
Winterwerp, J.C., de Boer, G.J., Greeuw, G., van Maren, D.S., 2012. Mud-induced wave damping and wave-induced liquefaction. Coast. Eng. 64, 102–112.
Winterwerp, J.C., van Kessel, T., van Maren, D.S., van Prooijen, B.C., 2021. Fine Sediment in Open Water, Advanced s Edition. Vol. 55 of Advanced Series on Ocean Engineering. WORLD SCIENTIFIC, Delft. https://doi.org/10.1142/12473.
Xie, X., Li, M., Ni, W., 2018. Roles of wind-driven currents and surface waves in sediment resuspension and transport during a tropical storm. J. Geophys. Res. Oceans 123 (11), 8638–8654.
Yang, S.L., Belkin, I.M., Belkina, A.I., Zhao, Q.Y., Zhu, J., Ding, P.X., 2003a. Delta response to decline in sediment supply from the Yangtze River: evidence of the recent four decades and expectations for the next half-century. Estuar. Coast. Shelf Sci. 57 (4), 689–699.
Yang, S.-L., Friedrichs, C.T., Shi, Z., Ding, P.-X., Zhu, J., Zhao, Q.-Y., 2003b. Morphological response of tidal marshes, flats and channels of the outer yangtze river mouth to a major storm. Estuaries 26, 1416–1425.
Yang, S., Li, H., Ysebaert, T., Bouma, T., Zhang, W., Wang, Y., Li, P., Li, M., Ding, P., 2008. Spatial and temporal variations in sediment grain size in tidal wetlands, yangtze delta: on the role of physical and biotic controls. Estuar. Coast. Shelf Sci. 77 (4), 657–671. https://www.sciencedirect.com/science/article/pii/S0272771407004921.
Yang, S., Shi, B., Bouma, T., Ysebaert, T., Luo, X., 2012. Wave attenuation at a salt marsh margin: a case study of an exposed coast on the yangtze estuary. Estuar. Coasts 35, 169–182.
Yang, S.L., Luo, X., Temmerman, S., Kirwan, M., Bouma, T., Xu, K., Zhang, S., Fan, J., Shi, B., Yang, H., et al., 2020. Role of delta-front erosion in sustaining salt marshes under sea-level rise and fluvial sediment decline. Limnol. Oceanogr. 65 (9), 1990–2009.
Yang, S., Bouma, T.J., Xu, K., Shi, B., Yang, H., Zhang, W., Luo, X., Li, P., Huang, Y., Tian, M., et al., 2023a. Storms dominate the erosion of the yangtze delta and southward sediment transport. Sci. Bull. 68 (6), 553–556.
Yang, S., Bouma, T.J., Xu, K., Shi, B., Yang, H., Zhang, W., Luo, X., Li, P., Huang, Y., Tian, M., et al., 2023b. Storms dominate the erosion of the yangtze delta and southward sediment transport. Sci. Bull. 68 (6), 553–556.
Zhang, M., Dai, Z., Bouma, T.J., Bricker, J., Townend, I., Wen, J., Zhao, T., Cai, H., 2021. Tidal-flat reclamation aggravates potential risk from storm impacts. Coast. Eng. 166 (February), 103868. https://doi.org/10.1016/j.coastaleng.2021.103868.
Zhu, Q., Yang, S., Ma, Y., 2014. Intra-tidal sedimentary processes associated with combined wave-current action on an exposed, erosional mudflat, southeastern Yangtze River Delta, China. Mar. Geol. 347, 95–106. https://linkinghub.elsevier.com/retrieve/pii/S0025322713002454.
Zhu, Q., van Prooijen, B.C., Wang, Z.B., Ma, Y.X., Yang, S.L., 2016. Bed shear stress estimation on an open intertidal flat using in situ measurements. Estuar. Coast. Shelf Sci. 182, 190–201.
Zhu, Q., van Prooijen, B.C., Wang, Z.B., Yang, S.L., 2017. Bed-level changes on intertidal wetland in response to waves and tides: a case study from the Yangtze River Delta. Mar. Geol. 385, 160–172. https://linkinghub.elsevier.com/retrieve/pii/S0025322717300130.
Zhu, Z., Vuik, V., Visser, P.J., Soens, T., van Wesenbeeck, B., van de Koppel, J., Jonkman, S.N., Temmerman, S., Bouma, T.J., 2020. Historic storms and the hidden value of coastal wetlands for nature-based flood defence. Nat. Sustain. 3 (10), 853–862.